JCI The Journal of Clinical Investigation

Visceral adipose NLRP3 impairs cognition in obesity via IL1R1 on Cx3cr1^{+} cells

De-Huang Guo, … , Babak Baban, Alexis M. Stranahan

J Clin Invest. 2020. https://doi.org/10.1172/JCI126078.

Research In-Press Preview **Immunology** **Neuroscience**

Induction of the inflammasome protein cryopyrin (NLRP3) in visceral adipose tissue (VAT) promotes release of the pro-inflammatory cytokine interleukin-1β (IL1β) in obesity. While this mechanism contributes to peripheral metabolic dysfunction, effects on the brain remain unexplored. These studies investigated whether visceral adipose NLRP3 impairs cognition by activating microglial interleukin-1 receptor 1 (IL1R1). After observing protection against obesity-induced neuroinflammation and cognitive impairment in NLRP3KO mice, we transplanted VAT from obese WT or NLRP3KO donors into lean recipients. Transplantation of VAT from a WT donor ($TRANS_{WT}$) increased hippocampal IL1β and impaired cognition, but VAT transplants from comparably obese NLRP3KO donors ($TRANS_{KO}$) had no effect. Visceral adipose NLRP3 was required for deficits in long-term potentiation (LTP) in transplant recipients, and LTP impairment in $TRANS_{WT}$ mice was IL1-dependent. Flow cytometric and gene expression analyses revealed that VAT transplantation recapitulated the effects of obesity on microglial activation and IL1β gene expression, and visualization of hippocampal microglia revealed similar effects in vivo. Inducible ablation of IL1R1 in CX3CR1-expressing cells eliminated cognitive impairment in mice with dietary obesity and in transplant recipients and restored immunoquiescence in hippocampal microglia. These results indicate that visceral adipose NLRP3 impairs memory via IL1-mediated microglial activation, and suggest that NLRP3-IL1β signaling may underlie correlations between visceral adiposity and cognitive impairment in humans.

Visceral adipose NLRP3 impairs cognition in obesity via IL1R1 on Cx3cr1+ cells

De-Huang Guo,[1] Masaki Yamamoto,[1] Caterina M. Hernandez,[2]† Hesam Khodadadi,[3] Babak Baban,[3,4] and Alexis M. Stranahan[1]*

[1]Department of Neuroscience and Regenerative Medicine, Medical College of Georgia, Augusta University, 1120 15th St, Augusta, GA 30912 USA

[2]Department of Pharmacology and Toxicology, Medical College of Georgia, Augusta University, 1120 15th St, Augusta, GA 30912 USA

[3]Department of Oral Biology, Medical College of Georgia, Augusta University, 1120 15th St, Augusta, GA 30912 USA

[4]Plastic Surgery Section, Department of Surgery, Medical College of Georgia, Augusta University, 1120 15th St, CL2118, Augusta, GA 30912 USA

*Corresponding Author:
Alexis M. Stranahan, Ph.D.
Department of Neuroscience and Regenerative Medicine
Medical College of Georgia, Augusta University
1120 15th St, CA3009, Augusta, GA 30912 USA
Ph: (706) 721-7885
Fax: (706) 434-7823
Email: astranahan@augusta.edu

†Current address:
Department of Pharmaceutical Sciences
Appalachian College of Pharmacy
1060 Dragon Road
Oakwood, VA 24631

Key words: Obesity; inflammation; microglia; learning and memory; hippocampus

Conflict of interest statement: The authors have declared no conflict of interest exists.

Abstract

Induction of the inflammasome protein cryopyrin (NLRP3) in visceral adipose tissue (VAT) promotes release of the pro-inflammatory cytokine interleukin-1β (IL1β) in obesity. While this mechanism contributes to peripheral metabolic dysfunction, effects on the brain remain unexplored. These studies investigated whether visceral adipose NLRP3 impairs cognition by activating microglial interleukin-1 receptor 1 (IL1R1). After observing protection against obesity-induced neuroinflammation and cognitive impairment in NLRP3KO mice, we transplanted VAT from obese WT or NLRP3KO donors into lean recipients. Transplantation of VAT from a WT donor ($TRANS_{WT}$) increased hippocampal IL1β and impaired cognition, but VAT transplants from comparably obese NLRP3KO donors ($TRANS_{KO}$) had no effect. Visceral adipose NLRP3 was required for deficits in long-term potentiation (LTP) in transplant recipients, and LTP impairment in $TRANS_{WT}$ mice was IL1-dependent. Flow cytometric and gene expression analyses revealed that VAT transplantation recapitulated the effects of obesity on microglial activation and IL1β gene expression, and visualization of hippocampal microglia revealed similar effects in vivo. Inducible ablation of IL1R1 in CX3CR1-expressing cells eliminated cognitive impairment in mice with dietary obesity and in transplant recipients and restored immunoquiescence in hippocampal microglia. These results indicate that visceral adipose NLRP3 impairs memory via IL1-mediated microglial activation, and suggest that NLRP3-IL1β signaling may underlie correlations between visceral adiposity and cognitive impairment in humans.

Obesity is a major public health issue, and while some overweight individuals are physiologically healthy, many develop serious pathological conditions. Obesity has a deleterious effect on the central nervous system (CNS), and these effects are not limited to classical metabolic circuits in the brain. Several studies have reported increased rates of age-related cognitive decline in human obesity (1-5) and atrophy of medial temporal lobe regions involved in memory, including the hippocampus (6-8). However, there are also negative reports that did not detect cognitive impairment or brain atrophy in obesity (9-11). Unresolved controversies surrounding obesity-induced cognitive impairment may be due to the use of weight/height ratio criteria that do not reflect differences in adipose tissue distribution. Individuals with the 'apple-shaped' distribution of body fat are at increased risk of developing diabetes (12). Visceral adiposity, as reflected by waist-to-hip ratio, is a stronger predictor of age-related cognitive impairment than body mass index (BMI) in humans (4, 13-14). Although consensus is emerging from human studies of dementia risk in obesity, work in animal models has yet to elucidate the specific mechanism linking visceral adiposity with cognitive impairment.

Deposition of visceral white adipose tissue (VAT) induces systemic inflammation and promotes the development of metabolic complications in obesity (15-16). Chronic lipid overload in visceral adipocytes is accompanied by release of damage-associated molecular patterns that attract monocyte precursors and induce their differentiation into adipose tissue macrophages (17). The inflammatory VAT microenvironment leads to formation of 'inflammasome' complexes that amplify innate immune responses in adipose tissue (18-19). NOD-like receptor family, pyrin domain containing 3 (NLRP3) is a core component of the inflammasome complex and visceral adipose NLRP3 induction promotes synthesis and release of the pro-inflammatory cytokine interleukin-1β (IL1β) in obesity (18). Whole-body *Nlrp3-/-* mice develop obesity but are protected

against high-fat diet-induced adipose tissue inflammation and insulin resistance (18-19). The *Nlrp3* null mutation also protects against cognitive deficits in aged mice and in mouse models of Alzheimer's disease (20-21), but the consequences of tissue-specific NLRP3 induction for neuroplasticity and neuroinflammation have yet to be elucidated.

We hypothesized that NLRP3 induction in visceral adipose tissue initiates microglial activation and cognitive impairment by increasing IL1β. Peripheral IL1β enters the CNS via saturable transporters at the blood-brain barrier (BBB; 22), and we reasoned that microglial interleukin-1 receptor 1 (*Il1r1*) activation would initiate an autocrine amplification loop similar to that previously reported in other disease models (23). This hypothesis was tested in a series of dietary obesity and visceral adipose tissue (VAT) transplantation experiments using *Nlrp3-/-* mutant mice and transgenic mice with inducible deletion of *Il1r1* in CX3CR1-expressing cells. Collectively, these data suggest that CNS immune cells detect and amplify peripheral IL1β generated following visceral adipose inflammasome activation, and that increases in CNS IL1β downstream of this cascade impair hippocampal synaptic plasticity and cognition in obesity. Our findings add to the growing literature on dynamic interactions between the brain and peripheral tissues, and provide further support for reinterpretation of immune privilege in the CNS.

Results

Resistance to obesity-induced neuroinflammation and cognitive dysfunction in NLRP3KO mice

Obesity promotes formation of inflammasome complexes in multiple tissues, including the brain (24), but the link between NLRP3 and obesity-induced cognitive impairment remains correlative at present. To determine whether the inflammasome protein NLRP3 is required for obesity-induced microglial activation and cognitive dysfunction, we maintained *Nlrp3-/-* mice

(KO) and Wt littermates on high-fat or low-fat diet (HFD, LFD). Consistent with previous reports (18-19), Wt and NLRP3KO mice gained comparable amounts of weight during the 12wk period (Figure 1A). The weight of the visceral, subcutaneous, and interscapular fat pads was also unaffected by genotype (Figure 1B). However, NLRP3KO mice were protected against increases in IL1β in VAT with HFD consumption (Figure 1C; $F_{1,12}$=16.83, p=0.002). Wt/HFD mice exhibited significant increases in circulating IL1β ($F_{1,12}$=8.05, p=0.02), but NLRP3KO/HFD mice did not differ from Wt/LFD (Figure 1C). Protection against IL1β accumulation was also observed in hippocampal lysates from NLRP3KO/HFD mice (Figure 1C; $F_{1,12}$=6.8, p=0.02), suggesting that resistance to obesity-induced peripheral inflammation in NLRP3KO mice extends to the CNS.

Microglia continuously sense and respond to molecular patterns in the local environment. Because microglial process retraction is a well-characterized response to inflammation, we visualized IBA1+ cells in the hippocampal dentate gyrus and analyzed their morphology. Microglia from Wt/HFD mice exhibited significant reductions in process length and complexity, indicated by lower numbers of intersections at 1-micron intervals around the soma (Figure 1D, $F_{1,14}$=6.61, p=0.02). Process length and complexity were unaffected in NLRP3KO/HFD mice, which did not differ from Wt/LFD (Figure 1D). There were no differences between Wt/LFD and NLRP3KO/LFD mice, indicating that NLRP3KO mice are resistant to HFD-induced microglial process retraction. Parallel visualization of the lysosomal marker CD68 revealed significant accumulation in IBA1+ microglia Wt/HFD mice, but not NLRP3KO/HFD mice (Figure 1D). Microglial CD68 accumulation was evident both qualitatively, and quantitatively, as determined by analysis of CD68+ puncta within regions of interest delineated by IBA1 labeling (Supplemental Figure 1A-B; $F_{1,14}$=13.47, p<0.001). Microglial CD68 accumulation occurs following phagocytosis, which could reflect protective or pathological responses (25). To

interpret changes in CD68 immunoreactivity, we performed immunofluorescence labeling for IBA1 and the classical activation marker MHCII. Consistent with previous studies (26), IBA1/MHCII double-positive cells were more frequent in Wt/HFD mice, relative to Wt/LFD (Supplemental Figure 1C-D; $F_{1,14}$=17.84, p<0.001). Colabeling for IBA1 and MHCII was rare in NLRP3KO/HFD mice, which did not differ from Wt/LFD (Supplemental Figure 1C-D).

To examine the role of NLRP3 in obesity-induced cognitive dysfunction, Wt and NLRP3KO mice were tested in the water maze after 12wk HFD or LFD. Wt/HFD mice had longer swim paths during acquisition training and exhibited deficits during the probe test, relative to Wt/LFD mice (Figure 1E; for acquisition, $F_{1,36}$=7.03, p=0.01; for probe, $F_{1,60}$=4.11, p=0.04). By contrast, NLRP3KO/HFD mice did not differ from Wt/LFD mice (Figure 1E). There was no effect of genotype in LFD mice, and all groups of mice performed similarly when swimming towards a visible platform (distance [m], mean±sem: Wt/LFD=5.8±1.1; Wt/HFD=5.9±0.7; KO/LFD=5.4±0.8; KO/HFD=5.3±1.0). After observing NLRP3-dependent deficits in learning and memory, we investigated changes in hippocampal synaptic plasticity using extracellular recordings in brain slices. Stimulation of medial perforant path afferents to the dentate gyrus revealed significant reductions in long-term potentiation (LTP) in Wt/HFD mice (Figure 1F; $F_{1,39}$=6.88, p=0.01). Deficits in LTP were mediated by NLRP3, as slices from NLRP3KO/HFD mice exhibited LTP that was comparable to Wt/LFD (Figure 1F), indicating that whole-body ablation of NLRP3 protects against obesity-induced microglial activation and maintains hippocampal plasticity in dietary obesity.

Visceral adipose NLRP3 increases hippocampal interleukin-1β

To determine whether NLRP3 induction in visceral fat regulates hippocampal IL1β, we transplanted VAT from Wt/HFD or NLRP3KO/HFD donors into lean Wt recipients (Figure 2A). Mice that received transplants from a Wt donor ($TRANS_{WT}$) or an NLRP3KO donor ($TRANS_{KO}$) were compared with sham-operated Wt mice maintained on LFD (LFD/SHAM) or HFD (HFD/SHAM). Visceral fat transplantation had no effect on body weight or glycemic control in recipients 2wk after surgery (Figure 2A-B), and there were no differences in transplant viability between Wt and NLRP3KO donors (Supplemental Figure 2A; n rejections: $TRANS_{WT}$, n=1; $TRANS_{KO}$, n=2). There was also no evidence of compensatory atrophy in resident fat pads from transplant recipients (Supplemental Figure 2B). Cleavage and release of IL1β is a prominent consequence of visceral adipose NLRP3 induction (18). Quantification of IL1β in hippocampus, VAT, and serum revealed parallel increases in $TRANS_{WT}$ and HFD/SHAM mice (Figure 2C). Increases in hippocampal IL1β were dependent on NLRP3, as $TRANS_{KO}$ mice had lower levels of IL1β than $TRANS_{WT}$ and did not differ from LFD/SHAM (Figure 2C; $F_{3,20}=6.42$, $p=0.003$). In the transplanted VAT, IL1β concentrations were significantly higher in transplants from $TRANS_{WT}$, relative to $TRANS_{KO}$ mice (Figure 2C; $t_{10}=7.34$, $p<0.001$). Dietary obesity increased IL1β concentrations in resident VAT, but these increases were not recapitulated by VAT transplantation (Figure 2C). qPCR analysis of *Il1b* mRNA in resident and transplanted VAT revealed similar trends, with increased expression in resident VAT from HFD/SHAM and in transplanted VAT from $TRANS_{WT}$ mice (Supplemental Figure 2C). Hippocampal *Il1b* induction was only observed following VAT transplantation, as mice that received subcutaneous adipose tissue (SAT) transplants from a Wt/HFD donor did not exhibit changes in *Il1b* mRNA (Supplemental Figure 2D). *Il1b* gene expression in SAT transplants did not differ from resident SAT in sham-operated mice (Supplemental Figure 2E), consistent with the relative

immunoquiescence reported in SAT, compared to VAT (16). Collectively, these data suggest that visceral adipose NLRP3 induction is required for increases in hippocampal IL1β after VAT transplantation.

Visceral adipose NLRP3 induction impairs hippocampal function

For analysis of NLRP3-mediated hippocampal dysfunction after VAT transplantation, groups of LFD mice received transplants from Wt or NLRP3KO donors with dietary obesity, as shown (Figure 2A). Two weeks after surgery, transplant recipients and sham-operated controls were tested in the water maze, Y-maze, and novel object recognition tasks. In the water maze, HFD/SHAM and $TRANS_{WT}$ mice had longer path lengths during acquisition training and spent less time in the target quadrant during the probe trial (Figure 2D; $F_{3,38}$=4.68, p=0.002). The effects of VAT transplantation were NLRP3-dependent, as $TRANS_{KO}$ mice had shorter path lengths than $TRANS_{WT}$ mice and did not differ from LFD/SHAM (Figure 2D). Changes in performance were not attributable to deficits in visuomotor navigation, as there were no differences when swimming toward a visible platform (distance [m], mean±sem: LFD/SHAM=7.29±0.74; HFD/SHAM=6.97±0.98; LFD/$TRANS_{WT}$=6.85±0.45; LFD/$TRANS_{KO}$= 6.47±0.99). Similar patterns were observed in the Y-maze, where HFD/SHAM and $TRANS_{WT}$ mice alternated less frequently than LFD/SHAM (Figure 2E; $F_{3,38}$=6.59, p=0.001). Alternation deficits were not observed in $TRANS_{KO}$ mice, which did not differ from LFD/SHAM (Figure 2E). In the object recognition test, HFD/SHAM and $TRANS_{WT}$ mice exhibited comparable reductions in novel object preference 30min after training with two identical objects (Figure 2F; $F_{3,44}$=6.46, p=0.01). Although within-subject reductions in novel object recognition over time were evident in all groups, $TRANS_{KO}$ mice spent more time exploring the novel object than $TRANS_{WT}$ mice,

and did not differ from LFD/SHAM (Figure 2F). Given that there were no differences in total object exploration (time with both objects [sec], mean±sem: LFD/SHAM=90.88±3.97; HFD/SHAM=81.50±4.71; LFD/TRANS$_{WT}$=90.28±3.94; LFD/TRANS$_{KO}$=85.03±4.99), the collective outcome of these experiments is consistent with a requirement for NLRP3 in VAT transplantation-induced memory deficits.

After behavioral testing, mice were euthanized for slice preparation and extracellular recording of dentate gyrus LTP. Slice preparations from HFD/SHAM and TRANS$_{WT}$ mice exhibited smaller increases in the field excitatory postsynaptic potential (fEPSP) one hour after tetanic stimulation (Figure 2G; $F_{3,41}$=6.41, p=0.001). By contrast, LTP in TRANS$_{KO}$ slices was significantly greater than TRANS$_{WT}$, and did not differ from LFD/SHAM (Figure 2G). There were no effects of diet or VAT transplantation on presynaptic paired-pulse plasticity or on the input/output ratio across a range of stimulation intensities (data not shown). To examine the role of hippocampal IL1 in LTP deficits, additional recordings were conducted in the presence of recombinant interleukin 1 receptor antagonist (IL1RA; 100μg/mL). Preincubation with IL1RA eliminated LTP deficits in HFD/SHAM and TRANS$_{WT}$ mice without influencing LTP in LFD/SHAM and TRANS$_{KO}$ mice (Figure 2H). Taken together, these results indicate that NLRP3 induction in VAT impairs cognition and suppresses LTP in an IL1-dependent manner.

Visceral adipose NLRP3 increases penetration of peripheral IL1β across the BBB

Coincident elevation of IL1β in VAT, serum, and hippocampus could reflect changes in blood-brain barrier (BBB) permeability, increased transport of peripheral IL1β into the CNS, or a signaling mechanism transduced by cerebrovascular cell populations. To determine whether dietary obesity and VAT transplantation regulate CNS exposure to peripheral IL1β, mice were

injected with 6xHistidine-tagged IL1β (6xHis-IL1β; 10 micrograms, IV) and the fluorescent tracer sodium fluorescein (NaFl, 10mg/kg IP; Supplemental Figure 3A). Hippocampal lysates from HFD/SHAM and $TRANS_{WT}$ mice exhibited greater penetration of 6xHis-IL1β, relative to LFD/SHAM (Supplemental Figure 3B; $F_{3,12}$=9.96, p=0.005). Increases in 6xHis-IL1β were NLRP3-dependent, as lysates from $TRANS_{KO}$ mice did not differ from LFD/SHAM (Supplemental Figure 3B). Changes in CNS penetration of exogenous IL1β were region-specific, as no group differences were observed in cortical, hypothalamic, or cerebellar lysates (Supplemental Figure 3C-E). These patterns are consistent with increased hippocampal exposure to peripheral IL1β, but could arise due to BBB breakdown or changes in transport. Obesity increases BBB permeability (27-28), and quantification of NaFl in hippocampal lysates from HFD/SHAM mice replicated this observation (Supplemental Figure 3F; $F_{3,12}$=10.94, p<0.001). However, increases in BBB permeability were not recapitulated by VAT transplantation (Supplemental Figure 3F), suggesting that CNS exposure to peripheral IL1β in transplant recipients may arise from changes in transport. Collectively, these data indicate that dietary obesity and VAT transplantation promote CNS exposure to peripheral IL1β via distinct mechanisms.

Cell type-specific responses to obesity and VAT transplantation

Neuroinflammation encompasses interactions between neurons, microglia, astroglia, and cerebrovascular cell populations. To gain insight into the cell type-specific effects of obesity and VAT transplantation, we isolated forebrain mononuclear cells (FMCs), astrocytes, and brain vascular endothelial cells (BVECs) for flow cytometry and analysis of gene expression. Because macrophage infiltration has been reported in both genetic and dietary obesity (29-30), we initially conducted immunophenotyping experiments in FMCs to determine their identity (Figure 3A). In

FMCs from HFD/SHAM mice, we observed significant increases in the proportion of CD45hi/Ly6Chi/CD11b+ cells, suggestive of macrophage infiltration (Figure 3B-C; $F_{3,16}$=7.75, p=0.001). However, this increase was not present in FMCs from VAT transplant recipients (Figure 3B-C). After observing that obesity, but not VAT transplantation, promotes macrophage infiltration into the brain parenchyma, we examined markers of classical activation in CD45low/Ly6Clow/CD11b+ microglia. Analysis of MHCII and TLR4 revealed evidence of microglial polarization in HFD/SHAM and $TRANS_{WT}$ samples (Figure 3D-E; for MHCII, $F_{3,16}$=4.94, p=0.02; for TLR4, $F_{3,20}$=5.95, p=0.02). Microglial induction of MHCII and TLR4 was not observed in $TRANS_{KO}$ mice, which did not differ from LFD/SHAM (Figure 3D-E), consistent with a requirement for NLRP3 in VAT transplantation-induced microglial activation.

Analysis of gene expression in FMCs, astrocytes, and BVECs revealed cell type-specific responses to obesity and VAT transplantation. Increases in *Il1b* mRNA were detected in FMCs and whole-hippocampal cDNA from HFD/SHAM and $TRANS_{WT}$ mice, relative to LFD/SHAM (Supplemental Figure 4A; for FMCs, $F_{3,28}$=7.75, p=0.003; for hippocampus, $F_{3,28}$=5.73, p=0.004). These effects were dependent on NLRP3, as $TRANS_{KO}$ samples exhibited reduced *Il1b* relative to $TRANS_{WT}$ and did not differ from LFD/SHAM (Supplemental Figure 4A). Quantification of additional pro-inflammatory cytokines revealed distinct responses to HFD or VAT transplantation. Specifically, *Il6* mRNA was increased in astrocytes and FMCs from HFD/SHAM mice, relative to LFD/SHAM (Supplemental Figure 4B; for FMCs, $F_{3,28}$=5.57, p=0.003; for astrocytes, $F_{3,28}$=3.65, p=0.03). Obesity also upregulated *Mcp1* expression in all cell types and in whole-hippocampal cDNA (Supplemental Figure 4C; for FMCs, $F_{3,28}$=3.51, p=0.03; for astrocytes, $F_{3,32}$=3.20, p=0.04; for BVECs, $F_{3,28}$=4.31, p=0.01; for hippocampus, $F_{3,28}$=5.02, p=0.006).

Transcriptomic studies of microglia and other CNS cell populations report low but detectable expression of *Il1r1* under normal physiological conditions (31-32). Upregulation of microglial *Il1r1* has also been reported in disease models and after chemogenetic depletion (33-34). We examined cellular patterns of *Il1r1* expression and immunoreactivity using immunofluorescence and qPCR (Supplemental Figure 4D-F). Paraformaldehyde-fixed microglia, astrocytes, and BVECs from normal mice were immunoreactive for IL1R1 and phenotype-specific antigens (Supplemental Figure 4D). Quantification of *Il1r1* mRNA revealed significant increases in FMCs from HFD/SHAM and $TRANS_{WT}$ mice (Supplemental Figure 4E-F; $F_{3,28}$=9.77, p=0.001). Taken together, these results implicate microglia as early detectors and potential amplifiers of visceral adipose-derived IL1β.

Obesity and VAT transplantation amplify microglial responses to IL1β

Peripheral macrophages and resident microglia exhibit sensitization in response to pro-inflammatory stimuli, including IL1β, which primes cells for autocrine amplification (33, 35; reviewed in 23). To examine whether microglia might amplify CNS responses to exogenous IL1β in obesity, we measured media cytokines and gene expression in FMCs from LFD/SHAM, HFD/SHAM, $TRANS_{WT}$, and $TRANS_{KO}$ mice. Cells from HFD/SHAM and $TRANS_{WT}$ mice had higher levels of media TNFα after stimulation with increasing concentrations of IL1β, relative to cells from LFD/SHAM mice (Figure 3F; $F_{3,48}$=2.98, p=0.006), indicative of sensitization. Visceral adipose NLRP3 was required for sensitization, as cells from $TRANS_{KO}$ mice did not differ from LFD/SHAM (Figure 3F). Sensitization of responses to IL1β were not explained by differences in viability, as there were no differences in cell survival after stimulation (Figure 3F). Priming of IL1β-stimulated gene expression was also evident based on lower thresholds for induction of

IL1b mRNA in FMCs from HFD/SHAM and $TRANS_{WT}$ mice (Figure 3G; $F_{3,48}$=9.18, p<0.001). By contrast, cells from $TRANS_{KO}$ mice exhibited IL1β-stimulated gene expression profiles that were comparable to LFD/SHAM (Figure 3G). When interpreted with the flow cytometry dataset (Figure 3B), these outcomes suggest that the mixed population of microglia and infiltrating macrophages in FMCs from HFD/SHAM mice and the relatively homogeneous population of microglia in FMCs from $TRANS_{WT}$ mice exhibit comparable sensitization and priming in response to IL1β. Moreover, the lack of sensitization and priming in primary microglia from $TRANS_{KO}$ mice is consistent with a requirement for NLRP3 in these effects.

Visceral adipose NLRP3 induction activates microglia in vivo

To investigate the consequences of VAT transplantation for microglia in the intact hippocampus, LFD/SHAM, HFD/SHAM, $TRANS_{WT}$, and $TRANS_{KO}$ mice were perfused 2wk after surgery for immunohistochemical visualization of the microglial marker IBA1 and the activation marker MHCII. Unbiased stereological quantification of total microglial number in the dentate molecular layer revealed no evidence of proliferation or cell loss with dietary obesity or VAT transplantation (Figure 4A). Activated microglia typically retract their processes, and we used process number as an indicator of activation state in these experiments. Dietary obesity and VAT transplantation were accompanied by increases in the number of 'Simple' microglia with $\leq$2 primary processes ($F_{3,24}$=7.14, p=0.005; Figure 4A), relative to LFD/SHAM. Microglial simplification was NLRP3-dependent, as counts of simple and complex ramified microglia did not differ between LFD/SHAM and $TRANS_{KO}$ mice (Figure 4A). 3D Reconstruction of IBA1+ cells revealed comparable reductions in process length and complexity in $TRANS_{WT}$ and HFD/SHAM mice (Figure 4B, $F_{3,16}$=9.04, p<0.001). Microglial process retraction was mediated by visceral

adipose NLRP3, as $TRANS_{KO}$ mice exhibited process lengths and Sholl profiles that did not differ from LFD/SHAM (Figure 4B). The effects of obesity and VAT transplantation were not limited to morphology, as visualization of the activation marker MHCII in IBA1+ cells revealed similar increases in colocalization in $TRANS_{WT}$ and HFD/SHAM mice (Figure 4C; $F_{3,16}$=12.84, p=0.002). By contrast, $TRANS_{KO}$ mice had significantly fewer IBA1/MHCII positive cells than $TRANS_{WT}$, and did not differ from LFD/SHAM, consistent with NLRP3-mediated microglial activation in vivo with obesity and VAT transplantation.

Generation and characterization of $CX3CR1^{creERT}/IL1R1^{fl/fl}$ transgenic mice

After observing correlated increases in IL1β, ex vivo sensitization, and microglial activation, we hypothesized that microglial IL1R1 activation might initiate these responses in dietary obesity. To address this question, we bred transgenic mice with inducible deletion of *Il1r1* under the *Cx3cr1* promoter (34). Although CX3CR1 is expressed by multiple monocyte lineages, differential turnover in resident microglia and peripheral myeloid cells enables selective manipulation of gene expression in the CNS >4wk after transgene induction (36). For additional insight into tissue-specific patterns of *Il1r1* expression in this model, groups of $CX3CR1^{creERT}/IL1R1^{fl/fl}$ mice (Tg) and nontransgenic littermates (nTg) were maintained on standard diet from weaning, with tamoxifen induction at 10wk old and tissue collection 1wk or 4wk post-induction (Supplemental Figure 5A). Amplification of genomic DNA from FMCs, spleen, VAT, and subcutaneous adipose tissue (SAT) using primers targeting the *Il1r1* deleted sequence revealed excision 1wk after tamoxifen in all tissues (Supplemental Figure 5B). However, at 4wk post-induction, the deleted sequence was only detectable in FMCs (Supplemental Figure 5B). qPCR analysis of *Il1r1* mRNA in the above tissues revealed parallel fluctuations in gene

expression (Supplemental Figure 5C-F). In FMCs from Tg mice, *Il1r1* mRNA was low or undetectable after >40 cycles of amplification (Supplemental Figure 5C). In spleen, VAT, and SAT, transient reductions in *Il1r1* mRNA were evident 1wk after induction, with complete recovery by 4wk (Supplemental Figure 5D-F), indicative of selective recombination in the brain one month after tamoxifen administration.

Brain-specific resistance to obesity-induced inflammation in CX3CR1^{creERT}/IL1R1$^{fl/fl}$ mice

To induce obesity, Tg mice and nTg littermates were maintained on HFD or LFD for 12wk, with induction during week 5 (Figure 5A). Tg and nTg mice gained similar amounts of weight and did not exhibit differences in glycemic control (Figure 5A-B). Obesogenic diet consumption increased the weight of the visceral and subcutaneous fat pads, but these effects were comparable in Tg and nTg mice (Figure 5C). Quantification of IL1β concentrations in hippocampus, VAT, and serum revealed brain-specific resistance to IL1β accumulation in Tg/HFD mice (Figure 5D). nTg/HFD mice exhibited increases in hippocampal IL1β ($F_{1,12}$=20.83, $p<0.001$), but hippocampal IL1β concentrations in Tg/HFD mice were comparable to nTg/LFD (Figure 5D). There was no effect of genotype on hippocampal IL1β in LFD mice, and HFD mice from both genotypes exhibited comparable increases in VAT and serum IL1β (Figure 5D; for serum, $F_{1,12}$=27.53, $p<0.001$; for VAT, $F_{1,12}$=23.66, $p<0.001$).

Increases in IL1β promote transmigration of peripheral monocytes into the CNS in other disease models (37), and after observing IL1R1-mediated increases in hippocampal IL1β, we examined whether Tg/HFD mice might be protected against obesity-induced macrophage infiltration (Figure 5E). Analysis of cell-surface IL1R1 expression in the SSClow/FSCmid/CD11b+/CD45+ population from FMCs and lysed whole blood upheld the

brain-specific recombination observed during characterization of the mouse line (Supplemental Figure 5). Both Tg/LFD and Tg/HFD mice exhibited comparable reductions in IL1R1 expression, relative to nTg mice (Figure 5F). Flow cytometric immunophenotyping of FMCs revealed accumulation of CD45hi/Ly6Chi cells in nTg/HFD mice ($F_{1,26}$=5.78, p=0.02). Increases were not observed in FMCs from Tg/HFD mice (Figure 5G), suggestive of a requirement for IL1R1 in obesity-induced macrophage infiltration.

The CD11b+/CD45hi/Ly6Chi population predominantly contains infiltrating macrophages (38-39), but the parent population of CD11b+/CD45hi cells is heterogeneous in its ontogeny and origin. The meninges, choroid plexus, and perivascular space contain populations of CNS border-associated macrophages (BAMs) generated during embryonic development (39-40). In the *Cx3cr1*^{creERT} line, long-lived BAMs exhibit persistent recombination >4wk post-induction (40), and to investigate responses in an analagous population, we analyzed intracellular IL1β fluorescence in the CD11b+/CD45hi/Ly6Clow cells. Reductions in IL1β mean fluorescence intensity (MFI) were evident in CD11b+/CD45hi/Ly6Clow cells from Tg mice (Figure 5H; $F_{1,8}$=31.3, p<0.001). Reductions were comparable in Tg/LFD and Tg/HFD mice, suggestive of diet-independent regulation (Figure 5H). Quantification of IL1β MFI in CD11b+/CD45low/Ly6Clow microglia identified non-overlapping responses to obesity and IL1R1 deletion. In nTg mice, IL1β fluorescence was weaker in microglia, relative to CD11b+/CD45hi/Ly6Clow cells, irrespective of diet (Figure 5H). Dietary obesity increased microglial IL1β MFI in nTg mice (Figure 5H; $F_{1,8}$=11.31, p=0.01), but not in Tg mice, suggestive of IL1R1-dependent mechanisms.

To determine whether differential regulation of IL1β might reflect differences in activation, we quantified cell-surface MHCII and TLR4 in CD11b+/CD45low/Ly6Clow microglia and in the

CD11b+/CD45hi/Ly6Clow population, which includes BAMs (38-40). In microglia, IL1R1 was required for obesity-induced inflammatory polarization (Figure 5I; for MHCII, $F_{1,14}$=17.83, p=0.008; for TLR4, $F_{1,14}$=15.18, p<0.001). Among CD45hi/Ly6Clow cells, IL1R1 deletion reduced MHCII and TLR4 expression in a diet-independent manner (Supplemental Figure 6A-B; for MHCII, $F_{1,14}$=5.67, p=0.03; for TLR4, $F_{1,14}$=11.28, p=0.005). Basal expression of MHCII and TLR4 was also higher among CD45hi/Ly6Clow cells, relative to microglia (Figure 5I and Supplemental Figure 6A-B). While these data do not capture the potential for dynamic interactions between the two cell populations over time, the outcome is suggestive of distinct responses to dietary obesity and IL1R1 deletion in microglia and brain macrophages.

We next visualized IBA1+ cells in the hippocampal dentate gyrus to examine the role of IL1R1 in obesity-induced microglial reactivity under intact conditions. Based on their morphology and location in the brain parenchyma, the IBA1+ cells sampled in these experiments likely represent resident microglia. Total process length and complexity were significantly reduced in nTg/HFD mice, but cells from Tg/HFD mice were indistinguishable from nTg/LFD controls (Figure 5J; $F_{1,12}$=5.56, p=0.03). Inducible ablation of IL1R1 also eliminated microglial accumulation of CD68+ puncta with dietary obesity (Figure 5J). Microglia from Tg/LFD and nTg/LFD mice exhibited comparable morphology and CD68 immunoreactivity (Figure 5J), consistent with a requirement for IL1R1 in obesity-induced microglial activation.

Activation of IL1R1 on CX3CR1-expressing cells underlies hippocampal dysfunction in obesity

After observing that IL1R1 was required for microglial IL1β activation, we examined the consequences of this cascade for hippocampal function. Transgenic mice and nTg littermates were maintained on HFD or LFD as shown (Figure 5A), with behavioral testing during weeks 10-

12. In the water maze, Tg/HFD mice were resistant to obesity-induced learning deficits, based on shorter path lengths relative to nTg/HFD mice, and intact performance during the probe trial (Figure 6A; for acquisition, $F_{1,44}$=7.22, p=0.01; for probe, $F_{1,44}$=12.62, p<0.001). There were no differences between nTg/LFD and Tg/LFD mice, and all groups performed comparably in the visible platform test (distance [m], mean±sem: nTg/LFD=5.87±0.4; nTg/HFD=5.62±0.7; Tg/LFD=6.20±0.5; Tg/HFD=5.2±0.6). Similar patterns were observed in the novel object preference paradigm, where Tg/HFD mice were protected against deficits in recognition memory 30min after training (Figure 6B; $F_{1,24}$=5.54, p=0.03). Differences in novel object preference were not explained by changes in total object exploration (time with both objects [sec], mean±sem: nTg/LFD = 83.5±5.4; nTg/HFD = 76.3±5.6; Tg/LFD = 87.1±4.9; Tg/HFD = 72.7±4.5), and all groups of mice exhibited within-subject decrements in object recognition over time (Figure 6B). In the Y-maze, IL1R1 expression was required for deficits in spatial recognition, based on reductions in alternation behavior in nTg/HFD, but not Tg/HFD mice (Figure 6C; $F_{1,25}$=5.44, p=0.005). In all paradigms, Tg/LFD mice did not differ from nTg/LFD controls, suggesting that microglial IL1R1 may be dispensable for hippocampus-dependent memory under basal conditions.

To examine the consequences of IL1R1-mediated neuroinflammation for hippocampal synaptic plasticity, we performed extracellular field potential recordings in hippocampal slices from Tg mice and nTg littermates after HFD or LFD. Induction of LTP revealed a pivotal role for IL1R1 in obesity-induced plasticity deficits (Figure 6D). nTg/HFD mice exhibited significant reductions in LTP magnitude, but Tg mice on HFD exhibited LTP that was comparable to nTg/LFD mice ($F_{1,44}$=8.86, p=0.008). Changes in LTP were not explained by alterations in the

input/output relationship (Figure 6E), or by changes in presynaptic paired-pulse depression (Figure 6F), suggestive of postsynaptic deficits following microglial IL1R1 activation.

While there is consensus that immune activation-induced elevations in IL1β impair LTP (41), the cellular targets for these effects remain poorly understood. To test the hypothesis that microglial IL1R1 activation underlies IL1β-mediated suppression of LTP, slices from nTg/LFD and Tg/LFD mice were pre-incubated with exogenous IL1β (1.0ng/mL) for 20min, with continued superperfusion of IL1β throughout recording (Figure 6G). Analysis of dendritic field potentials 1hr after tetanic stimulation revealed significant impairment of LTP in nTg/LFD slices (t_{14}=5.77, $p<0.001$). LTP deficits were not observed in slices from Tg/LFD mice, implicating microglial IL1R1 activation as a mechanism for IL1β-mediated LTP impairment. In support of this interpretation, co-application of the microglial inhibitor minocycline (20μM) and IL1β blocked LTP deficits in slices from nTg/LFD mice without influencing LTP in Tg/LFD slices (Figure 6G). Taken together, these results are consistent with an obligatory role for IL1R1 signaling among CX3CR1-expressing cells in IL1β-mediated synaptic dysfunction.

Direct evidence for autocrine amplification of IL1β after VAT transplantation

To investigate the role of IL1R1 in neuroinflammation after VAT transplantation, Tg mice and nTg littermates received tamoxifen one month before sham operation or VAT transplantation surgery (Figure 7A). Two weeks after surgery, mice were fasted for IPGTT before being euthanized for isolation of FMCs or immunohistological analysis of IBA1+ microglia. There was no effect of genotype on weight gain after surgery (Figure 7A), and there were no changes in glycemic control in Tg mice (Figure 7B). Analysis of IL1β concentrations in hippocampus, serum, and VAT revealed brain-specific protection in Tg mice that received VAT transplants

(Tg/TRANS). Hippocampal IL1β concentrations were elevated in nTg/TRANS mice, but Tg/TRANS mice were indistinguishable from sham-operated mice (Figure 7C; $F_{1,20}$=6.38, p=0.02). Transplant recipients had increased serum IL1β, relative to sham-operated mice, but increases in circulating IL1β were unaffected by genotype (Figure 7C). Concentrations of IL1β were significantly higher in the transplanted VAT, relative to resident VAT, but there was no effect of recipient genotype on IL1β in either set of samples (Figure 7C). Fluctuations in adipose IL1β protein concentrations were paralleled by changes in *Il1b* gene expression, which was significantly elevated in transplanted VAT independently of recipient genotype (Figure 7D). After observing protection against hippocampal IL1β accumulation in Tg/TRANS mice, we analyzed microglial morphology and MHCII induction. VAT transplantation increased the number of IBA1/MHCII double-positive cells in nTg mice, but not in Tg mice (Figure 7E; $F_{1,16}$=24.52, p<0.001). Changes in MHCII immunoreactivity were accompanied by IL1R1-mediated reductions in microglial process length and complexity (Figure 7E; $F_{1,16}$=8.85, p=0.008). Collectively, these results indicate that IL1R1 expression among CX3CR1-expressing cells is required for neuroinflammation following surgical increases in visceral fat.

After observing an obligatory role for IL1R1 in hippocampal IL1β accumulation, we investigated the potential requirement for IL1R1 in autocrine amplification of IL1β ex vivo. Analysis of gene expression in FMCs after stimulation with increasing concentrations of IL1β revealed IL1R1-mediated priming in transplant recipients (Figure 7F). Cells from nTg/TRANS mice had lower thresholds for induction of *IL1b* mRNA, but cells from Tg/TRANS mice were comparable to nTg/SHAM (Figure 7F; $F_{1,20}$=48.28, p<0.01). Priming of gene expression was accompanied by IL1R1-mediated sensitization, based on increases in media TNFα in cells from nTg/TRANS, but not Tg/TRANS mice (Figure 7G; $F_{1,20}$=19.63, p=0.002). Changes in

sensitization and priming were not attributable to differential cell survival, as there were no group differences based on formazan cleavage assay (Figure 7G). The effect of genotype was only evident in transplant recipients, as cells from Tg/SHAM mice did not differ from nTg/SHAM (Figure 7F-G). Taken together, these patterns are consistent with IL1R1-mediated autocrine amplification of *IL1b* expression following VAT transplantation.

Protection against obesity-induced microglial activation in CX3CR1^{creER}/IL1R1$^{fl/fl}$ mice

Microglia interact with neurons via receptor-mediated signaling, alone or in concert with physical interactions with synaptic terminals (25, 42-43). We previously reported that dietary obesity disrupts the organization of microglial processes around hippocampal synaptic terminals (26). To investigate whether VAT transplantation might recapitulate these effects and examine the potential contributions of IL1R1, Tg mice were crossed with the Thy1-eGFP(S) line to generate CX3CR1^{creERT}/IL1R1$^{fl/fl}$ with endogenous fluorescence in dentate granule neurons (Figure 8A-B). Semi-automated detection and quantification of dendritic spines revealed reductions in total dendritic spine density after VAT transplantation (Figure 8A; $F_{1,21}$=10.92, p=0.003). These effects were primarily attributable to loss of thin spines and were mediated by IL1R1 activation among CX3CR1-expressing cells (Figure 8A-B; $F_{1,21}$=9.01, p=0.007). Parallel visualization of IBA1 revealed preferential localization of microglial processes at mushroom spines, relative to other morphologies, in all groups of mice (Figure 8B; # spines sampled per animal, mean$\pm$sem=551$\pm$75.2). This pattern was further amplified by VAT transplantation in nTg/TRANS mice ($F_{1,21}$=10.08, p=0.004). The effects of VAT transplantation on microglial apposition at mushroom spines were IL1R1-dependent, as Tg/TRANS mice had similar proportions of mushroom spines with perisynaptic microglial processes, relative to nTg/SHAM

(Figure 8B). IL1R1-mediated perturbation of microglia-synapse relationships was only evident after VAT transplantation, as Tg/SHAM mice did not differ from nTg/SHAM in terms of spine density or microglial localization (Figure 8A-B). Collectively, these results are consistent with a multifaceted role for IL1R1 in regulating microglia/synapse interactions following surgical increases in visceral fat.

To examine the functional consequences of IL1R1-mediated changes in microglia/synapse relationships, we performed extracellular recordings in brain slices. Dentate gyrus LTP was significantly reduced in slices from nTg/TRANS, but not in Tg/TRANS mice (Figure 8C; $F_{1,40}$=10.56, p=0.003). Presynaptic paired-pulse plasticity was unaffected at interpulse intervals ranging from 50msec to 1sec (Figure 8D), and comparison of the input/output curve over a range of stimulus intensities revealed no effect of genotype or surgery (Figure 8E). Analysis of hippocampus-dependent memory in the water maze revealed that IL1R1 was required for memory deficits after VAT transplantation (Figure 8F). Tg/TRANS mice had shorter swim paths than nTg/TRANS mice during acquisition training and performed on par with nTg/SHAM during the probe trial (Figure 8F; for acquisition, $F_{3,56}$=9.09, p=0.003; for probe, $F_{1,56}$=5.55, p=0.03). There were no differences between nTg/SHAM and Tg/SHAM during acquisition training, and there was no effect of genotype or VAT transplantation on navigation toward the visible platform (distance [m]; mean$\pm$sem, nTg/SHAM = 6.78 $\pm$ 1.25; nTg/TRANS = 7.27 $\pm$ 0.98; Tg/SHAM = 6.46 $\pm$ 1.49; Tg/TRANS = 7.21 $\pm$ 0.77). Ablation of IL1R1 also eliminated deficits in spontaneous alternation in the Y-maze after VAT transplantation (Figure 8G; $F_{1,38}$=4.55, p=0.04). There were no differences in alternation between nTg/SHAM and Tg/SHAM mice (Figure 8G). In the object recognition task, Tg/TRANS mice performed significantly better than nTg/TRANS mice at the 30min post-training timepoint (Figure 8H; $F_{3,43}$=9.52, p=0.005).

There were no differences in object recognition between nTg/SHAM and Tg/SHAM, and all groups of mice exhibited within-subject reductions in novel object preference over time (Figure 8H). Taken together, these data indicate that IL1R1 activation among CX3CR1-expressing cells underlies VAT transplantation-induced deficits in hippocampus-dependent memory.

Discussion

While there is consensus that obesity elicits pro-inflammatory responses in peripheral tissues, interpretation of similar changes in the brain is complicated by longstanding assumptions regarding immune privilege in the nervous system. The current studies add to a growing body of work challenging these assumptions by demonstrating that NLRP3 inflammasome activation in visceral adipose tissue impairs cognition in obesity. These effects were mediated by activation of IL1R1 among CX3CR1-expressing cells, which detect and amplify IL1β in the brain. Given that aging, AD, and obesity are associated with NLRP3 induction and local inflammation in multiple tissues, including the CNS (20-21, 24), it is surprising that tissue-specific requirements for NLRP3 remain poorly understood. To our knowledge, the VAT transplantation studies in this report represent the first regionally selective manipulation of NLRP3 to examine tissue-specific regulation of synaptic plasticity and cognition.

Visceral adipose NLRP3 induction promotes caspase 1-mediated cleavage of pro-IL1β, leading to release of mature IL1β from adipose tissue macrophages (18, 44-45). Multiple lines of evidence in this report suggest that exposure to peripherally generated IL1β initiates local amplification by brain-resident immune cells, similar to that reported following intracerebroventricular IL1β injections and in experimental autoimmune encephalomyelitis (33, 46). However, it is also possible that CNS border-associated macrophages (BAMs) in the

meninges and perivascular space could instigate or oppose parenchymal responses to IL1β. Long-lived BAMs exhibit recombination at extended timepoints after induction in the CX3CR1^{creERT} line (40), and interactions between BAMs and CSF immune cells were previously shown to regulate cognition (47). In light of these patterns, it is possible that obesity-induced cognitive deficits could arise due to IL1R1 activation on BAMs, alone or in concert with responses among resident microglia. Under one potential scenario, IL1R1 activation would promote synthesis and release of IL1β by BAMs, which would reach the hippocampus directly by volume transmission, or indirectly via paracrine signaling interactions with adjacent cells (46, 48). Although the indirect hypothesis cannot be ruled out, the timeframe for changes in hippocampal synaptic plasticity following *ex vivo* manipulation of IL1 signaling suggests a more proximal interaction between CX3CR1-expressing cells and synaptic terminals. Perivascular macrophages represent the most likely subpopulation of BAMs for these effects, given their parenchymal location and instigatory role in neuroinflammation following peripheral infection (49-50). However, in obesity peripheral inflammation develops more slowly than in models of acute infection, and the contributions of perivascular macrophages to chronic (neuro)inflammation are less certain. The difficult questions surrounding the origins of neuroinflammation in obesity are emblematic of larger gaps in knowledge related to CNS immune privilege and the degree of interaction between parenchymal cells and circulating factors. Although the subpopulation of CX3CR1-expressing cells that initiates obesity-induced cognitive dysfunction remains to be determined, the current report clearly implicates IL1R1 activation in brain-resident immune cells as a link between visceral adipose NLRP3 induction and cognitive impairment.

Within the CNS, IL1R1 is highly expressed among vascular endothelial cells, with lower but detectable expression in microglia, astrocytes, and neurons (31-34, 51-53). Microglial IL1R1

expression is upregulated following chemogenetic depletion and in animal models of chronic inflammation (33-34), consistent with a central role for IL1 signaling in repopulation and resolution of neuroinflammation. The downstream effects of IL1R1 activation in the brain are determined by cell type-specific expression of splice variants for the IL1 receptor accessory protein (AcP). The AcP variant expressed by glia is identical to the co-receptor expressed in peripheral tissues, while the AcPb variant is exclusively expressed by neurons (54-55). Both receptors have homologous extracellular regions, but the AcPb variant is unable to recruit the adapter protein MyD88, which is required for downstream induction of pro-inflammatory signaling cascades (23). Consistent with this, exogenous IL1β recruits NFκb-mediated transcriptional responses in glial cultures, but not in primary neurons (52). Interestingly, aging is accompanied by neuronal induction of the pro-inflammatory AcPb variant (56), suggesting that chronic exposure to low-level inflammation might reprogram neuronal IL1RAcP expression in other disease states. While the potential contributions of neuronal ILRAcP reconfiguration remain unexplored in obesity, it is tempting to speculate that a switch in AcP splice variant expression might occur downstream of local amplification of IL1β among CX3CR1-expressing cells in these experiments.

An extensive body of work indicates that exposure to levels of IL1β seen in chronic inflammatory diseases impairs hippocampal synaptic plasticity and cognition (57-59; reviewed in ref.41). The relationship between IL1β and hippocampal synaptic function is biphasic, with enhancement of synaptic plasticity following picomolar stimulation and deficits occurring after exposure to higher concentrations (54, 58, 60). Consistent with a facilitative role for low-level IL1R1 activation in synaptic physiology, whole-body IL1R1 knockout mice exhibit deficits in hippocampus-dependent memory and LTP (61). The dose-dependent effects of IL1β on

hippocampal synaptic plasticity have been interpreted as reflecting direct actions on neurons, but this assumption has yet to be adequately tested with modern cell type-specific approaches. In this report, we observed that ablation of IL1R1 among CX3CR1-expressing cells protects against IL1β-mediated deficits in LTP. The effects observed in normal-weight IL1R1Tg mice were similar to the protective effects of preincubation with minocycline, a broad-spectrum tetracycline antibiotic used experimentally to inhibit microglial activation (62-63). Taken together, these results suggest that the biphasic relationship between IL1β and hippocampal synaptic plasticity may reflect activation of IL1R1 on different cell types, with opposing consequences for memory and cognition.

Microglia regulate neuronal function indirectly by clearing dead cells and extracellular debris, and directly by releasing signaling molecules that support or suppress neuroplasticity (36). Interactions between microglia and neurons may also involve physical interposition of microglial processes between pre- and post-synaptic structures, alone or in concert with microglial internalization of synaptic terminals (25, 42). It is unlikely that microglial localization at mushroom spines in this report reflects synaptic stripping, given that a recent large-scale analysis of hippocampal dendritic spines using correlated light and electron microscopy revealed no evidence of postsynaptic internalization (43). VAT transplantation was associated with IL1R1-mediated loss of thin spines in these studies, consistent with our previously published ultrastructural studies in genetically obese db/db mice (64). However, any potential relationship between loss of thin spines and IL1R1-mediated microglial activation remains speculative at present. Understanding and manipulating glial interactions with synapses and circuits is a formidable challenge with the potential to uncover novel strategies for prevention and treatment of neurological disease.

In humans, there is consensus that insulin resistance is accompanied by increased risk of cognitive decline (65). By contrast, data from studies of BMI and cognition are often conflicting, with reports of increased risk (1-5), decreased risk (9), or negative findings (10-11, 66). The results of the current study could potentially underlie the reported associations between visceral adiposity and cognitive decline in human studies (4, 13-14). Given that a growing literature from longitudinal and twin studies supports a potential link between visceral adiposity and age-related cognitive decline, intervention studies may be warranted to prevent or attenuate risk. While there is a clear positive effect of lifestyle interventions, including the Mediterranean diet and exercise (67-68), long-term compliance can be difficult to achieve for most individuals. Surgical interventions such as Roux-en-Y gastric bypass, vertical banded gastroplasty, and laparoscopic adjustable gastric banding have begun to receive greater attention with respect to postoperative changes in memory and cognition. In a recent meta-analysis, significant improvements in attention, mood, and executive function were detected after bariatric surgery in morbidly obese patients (69). Cognitive improvements were independent of reductions in BMI, while reductions in circulating markers of inflammation were correlated with cognitive change in some, but not all studies (70-71). Bariatric surgery is sometimes performed together with surgical removal of fat from the visceral omentum (omentectomy). Although most studies did not report any metabolic improvements following omentectomy alone or with concurrent gastric bypass surgery (72-73; reviewed in ref.74), omentectomy has not been studied with respect to the regulation of cognition in humans. For mild to moderate obesity, surgical interventions will generate more risk than reward, even in the context of long-term vulnerability to age-related cognitive decline. However, studying brain circuits that respond to weight loss surgery could uncover novel targets for

noninvasive modulation using transcranial magnetic stimulation and other emerging technologies.

Materials and Methods

Animals and diets

To induce obesity, male mice were maintained on high-fat diet (HFD; Research Diets D12492) or low-fat diet (LFD; D12450) beginning at 8wk old. Wt and NLRP3KO mice (Jax strain #021302) were obtained from Jackson Labs or bred in-house for these experiments. Mice with inducible ablation of interleukin 1 receptor 1 in CX3CR1-expressing cells ($CX3CR1^{creER}/IL1R1^{fl/fl}$) were generated by crossing IL1R1flox mice (ref.34; kindly provided by Dr. Ari Waisman, University of Mainz, Mainz, Germany) with $CX3CR1^{creER}$ mice purchased from Jackson Labs (strain #021160). For some experiments, $CX3CR1^{creER}/IL1R1^{fl/fl}$ transgenic mice were crossed with the Thy1-eGFP(S) line (Jackson labs strain #011070; breeding pairs donated by Dr. Lin Mei, Augusta University, Augusta, GA USA) to generate Tg mice with endogenous fluorescence in the dendritic arbor of dentate granule neurons. Transgenic mice and nTg littermates were administered tamoxifen (2mg in 0.2mL corn oil, PO) 3x every 48hr. For additional description of housing conditions, genotyping, and animal care, please see Supplemental Experimental Procedures.

Fat transplantation and determination of transplant viability

For WAT transplantation, the epididymal or inguinal fat pads were removed and trimmed to 300mg before transplantation into the peritoneal cavity of recipients, as reported previously

(75). Transplants were collected at euthanasia for histological verification of transplant viability as described in Supplemental Experimental Procedures.

Behavioral testing

Testing in the Y-maze and novel object preference tasks was carried out as described (26, 29). Hippocampus-dependent memory was assessed using the water maze, as reported previously (76-77). Data acquisition was carried out blind to experimental condition, with the exception of the visually evident phenotype in HFD mice. Data analysis was carried out blind in Anymaze software.

BBB permeability and IL1β transport

Mice were injected with 6xHistidine-tagged recombinant IL1β (1.0 micrograms, IV; USBio) and the fluorescent tracer sodium fluorescein (NaFl; 10mg/kg, IP) before being euthanized by transcardial perfusion with saline, as described (28). The dose and route of administration for His-IL1β was selected based on the absence of acute IL1-mediated effects on BBB permeability (78). Detection and quantification of NaFl followed published methodology (28).

Enzyme-linked immunosorbent assay and western blotting

Protein extraction and quantification of IL1β and TNFα by ELISA followed published protocols (79; see Supplemental Experimental Procedures). Methods for SDS-PAGE and western blotting were modified from published protocols (28, 75) and are described in Supplemental Experimental Procedures.

Immunofluorescence, confocal microscopy, and morphological analysis

For details regarding immunofluorescence reactions, see Supplemental Experimental Procedures. Images were acquired on a Zeiss 780 multiphoton microscope and analyzed by a blinded experimenter. For cell sampling and analysis, see Supplemental Experimental Procedures.

Cell isolation and ex vivo stimulation

Cells were isolated according to published protocols (28) before labeling with conjugated antibodies for flow cytometry or frozen for gene expression endpoints (see Supplemental Experimental Procedures). Methods for ex vivo stimulation experiments were modified from published studies (75, 79) and are described in Supplemental Experimental Procedures.

Flow cytometry

For cell-surface markers, immunophenotyping was carried out as described (29; see Supplemental Experimental Procedures). For intracellular flow cytometry, live cells were incubated with conjugated antibodies against CD45, Ly6C, and CD11b before fixation and permeabilization using commercial reagents (Affymetrix eBioscience). Cells were then washed and incubated with primary antibodies for intracellular detection of IL1β (Santa Cruz Biotechnology). Viable cells were visibly differentiated from debris by size gating and positivity for specific antibodies using a BD LSRII flow cytometer (BD Biosciences). Single stains were used to set compensation and isotype controls were used to determine the level of nonspecific binding. Analysis was carried out in FlowJo version 11.0 (BD Bioscience) or InCyte software (Millipore, Temecula, CA).

RNA isolation and qPCR

Total RNA extraction and cDNA synthesis followed published methodology (28, 64; see Supplemental Experimental Procedures).

Hippocampal slice preparation and electrophysiology

Hippocampal slice preparation and extracellular recording were carried out as described (28-29, 75; see Supplemental Experimental Procedures).

Statistics

For comparisons between LFD/SHAM, HFD/SHAM, $TRANS_{WT}$, and $TRANS_{KO}$ mice, data were analyzed with one-way ANOVA or one-way repeated measures ANOVA followed by Tukey's HSD post hoc. For repeated-measures endpoints, data were analyzed using repeated-measures ANOVA and Tukey's HSD post hoc. For experiments comparing the effects of HFD or VAT transplantation in $CX3CR1^{creERT2}/IL1R1^{fl/fl}$ transgenic mice (Tg) and nontransgenic littermates, single-endpoint datasets were analyzed using 2x2 ANOVA (diet x genotype or surgery x genotype) with Tukey's HSD post hoc. For repeated-measures endpoints, data were analyzed using 2x2 repeated-measures ANOVA with Tukey's HSD post hoc. Where appropriate, the Greenhouse-Geisser correction was applied for heterogeneity of variance. For all analyses, statistical significance was carried out in Graphpad version 8.0 (Prism, Carlsbad, CA) with significance at $p<0.05$.

Study Approval

All experiments followed NIH guidelines and were approved by the Animal Care and Use Committee at the Medical College of Georgia.

Author contributions: AMS and DHG designed research studies; all authors were directly involved in conducting experiments, acquiring data, analyzing data, and writing the manuscript.

Acknowledgements: These studies were supported by grants from the National Institutes of Health to A.M.S. (K01DK100616, R03DK101817, R01DK110586). We are grateful to Dr. Ari Waisman and Dr. Sergey Grivennikov for providing breeding pairs of IL1R1flox mice, and to Dr. Lin Mei for breeding pairs of Thy1-eGFP(S) mice. Experiments involving RNA extraction from paraffin-embedded samples were carried out with assistance from the Genomics Core facility at Augusta University.

References

1. Xu W, Qiu C, Gatz M, Pedersen NL, Johansson B, Fratiglioni L. Mid- and late-life diabetes in relation to the risk of dementia: a population-based twin study. *Diabetes*. 2009;58(1):71-7.
2. Xu W, Caracciolo B, Wang HX, et al. Accelerated progression from mild cognitive impairment to dementia in people with diabetes. *Diabetes*. 2010;59(11):2928-35.
3. Xu WL, Atti AR, Gatz M, Pedersen NL, Johansson B, Fratiglioni L. Midlife overweight and obesity increase late-life dementia risk: a population-based twin study. *Neurology*. 2011;76(18):1568-74.
4. Whitmer RA, Gustafson DR, Barrett-Connor E, Haan MN, Gunderson EP, Yaffe K. Central obesity and increased risk of dementia more than three decades later. *Neurology*. 2008;71(14):1057-64.
5. Sabia S, Kivimaki M, Shipley MJ, Marmot MG, Singh-Manoux A. Body mass index over the adult life course and cognition in late midlife: the Whitehall II Cohort Study. *Am J Clin Nutr*. 2009;89(2):601-7.

6. Roriz-Cruz M, Rosset I, Wada T, et al. Cognitive impairment and frontal-subcortical geriatric syndrome are associated with metabolic syndrome in a stroke-free population. *Neurobiol Aging*. 2007;28(11):1723-36.
7. Wu W, Brickman AM, Luchsinger J, et al. The brain in the age of old: the hippocampal formation is targeted differentially by diseases of late life. *Ann Neurol*. 2008;64(6):698-706.
8. Ho AJ, Raji CA, Becker JT, et al. Obesity is linked with lower brain volume in 700 AD and MCI patients. *Neurobiol Aging.* 2010;31(8):1326-39.
9. van den Berg E, Biessels GJ, de Craen AJ, Gussekloo J, Westendorp RG. The metabolic syndrome is associated with decelerated cognitive decline in the oldest old. *Neurology*. 2007;69(10):979-85.
10. Sturman MT, de Leon CF, Bienias JL, Morris MC, Wilson RS, Evans DA. Body mass index and cognitive decline in a biracial community population. *Neurology*. 2008;70(5):360-7.
11. Xiong GL, Plassman BL, Helms MJ, Steffens DC. Vascular risk factors and cognitive decline among elderly male twins. *Neurology*. 2006;67(9):1586-91.
12. Kanneganti TD, Dixit VD. Immunological complications of obesity. *Nat Immunol*. 2012;13(8):707-12.
13. Elias MF, Elias PK, Sullivan LM, Wolf PA, D'Agostino RB. Obesity, diabetes and cognitive deficit: The Framingham Heart Study. *Neurobiol Aging*. 2005;26 Suppl 1:11-6.
14. Kamogawa K, Kohara K, Tabara Y, et al. Abdominal fat, adipose-derived hormones and mild cognitive impairment: the J-SHIPP study. *Dement Geriatr Cogn Disord*. 2010;30(5):432-9.
15. Rosen ED, Spiegelman BM. What we talk about when we talk about fat. *Cell*. 2014;156(1-2):20-44.
16. Osborn O, Olefsky JM. The cellular and signaling networks linking the immune system and metabolism in disease. *Nat Med*. 2012;18(3):363-74.
17. Chawla A, Nguyen KD, Goh YP. Macrophage-mediated inflammation in metabolic disease. *Nat Rev Immunol*. 2011;11(11):738-49.
18. Vandanmagsar B, Youm YH, Ravussin A, et al. The NLRP3 inflammasome instigates obesity-induced inflammation and insulin resistance. *Nat Med*. 2011;17(2):179-88.
19. Iyer SS, Pulskens WP, Sadler JJ, et al. Necrotic cells trigger a sterile inflammatory response through the Nlrp3 inflammasome. *Proc Natl Acad Sci U S A*. 2009;106(48):20388-93.
20. Youm YH, Grant RW, McCabe LR, et al. Canonical Nlrp3 inflammasome links systemic low-grade inflammation to functional decline in aging. *Cell Metab*. 2013;18(4):519-32.
21. Heneka MT, Kummer MP, Stutz A, et al. NLRP3 is activated in Alzheimer's disease and contributes to pathology in APP/PS1 mice. *Nature*. 2013;493(7434):674-8.
22. Banks WA, Kastin AJ. The interleukins-1 alpha, -1 beta, and -2 do not acutely disrupt the murine blood-brain barrier. *Int J Immunopharmacol*. 1992;14(4):629-36.

23. Weber A, Wasiliew P, Kracht M. Interleukin-1 (IL-1) pathway. *Sci Signal*. 2010;3(105):cm1.

24. Sobesky JL, D'Angelo HM, Weber MD, et al. Glucocorticoids Mediate Short-Term High-Fat Diet Induction of Neuroinflammatory Priming, the NLRP3 Inflammasome, and the Danger Signal HMGB1. *eNeuro*. 2016;3(4). pii: ENEURO.0113-16.2016.

25. Salter MW, Stevens B. Microglia emerge as central players in brain disease. *Nat Med*. 2017;23(9):1018-1027.

26. Hao S, Dey A, Yu X, Stranahan AM. Dietary obesity reversibly induces synaptic stripping by microglia and impairs hippocampal plasticity. *Brain Behav Immun*. 2016;51:230-9.

27. Kanoski SE, Zhang Y, Zheng W, Davidson TL. The effects of a high-energy diet on hippocampal function and blood-brain barrier integrity in the rat. *J Alzheimers Dis*. 2010;21(1):207-19.

28. Yamamoto M, Guo DH, Hernandez CM, Stranahan AM. Endothelial Adora2a Activation Promotes Blood-Brain Barrier Breakdown and Cognitive Impairment in Mice with Diet-Induced Insulin Resistance. J Neurosci. 2019 May 22;39(21):4179-4192.

29. Stranahan AM, Hao S, Dey A, Yu X, Baban B. Blood-brain barrier breakdown promotes macrophage infiltration and cognitive impairment in leptin receptor deficient mice. *J Cereb Blood Flow Metab*. 2016;36(12):2108-2121.

30. Buckman LB, Hasty AH, Flaherty DK, et al. Obesity induced by a high-fat diet is associated with increased immune cell entry into the central nervous system. *Brain Behav Immun*. 2014;35:33-42.

31. Zhang Y, Chen K, Sloan SA, et al. An RNA-sequencing transcriptome and splicing database of glia, neurons, and vascular cells of the cerebral cortex. *J Neurosci*. 2014;34(36):11929-47.

32. Li Q, Cheng Z, Zhou L, et al. Developmental Heterogeneity of Microglia and Brain Myeloid Cells Revealed by Deep Single-Cell RNA Sequencing. *Neuron*. 2019;101(2):207-223.

33. Zhang CJ, Jiang M, Zhou H, et al. TLR-stimulated IRAKM activates caspase-8 inflammasome in microglia and promotes neuroinflammation. *J Clin Invest*. 2018;128(12):5399-5412.

34. Bruttger J, Karram K, Wörtge S, et al. Genetic Cell Ablation Reveals Clusters of Local Self-Renewing Microglia in the Mammalian Central Nervous System. *Immunity*. 2015;43(1):92-106.

35. Toda Y, Tsukada J, Misago M, Kominato Y, Auron PE, Tanaka Y. Autocrine induction of the human pro-IL-1beta gene promoter by IL-1beta in monocytes. J Immunol. 2002;168(4):1984-91.

36. Parkhurst CN, Yang G, Ninan I, et al. Microglia promote learning-dependent synapse formation through brain-derived neurotrophic factor. *Cell*. 2013;155(7):1596-609.

37. Paré A, Mailhot B, Lévesque SA, et al. IL-1β enables CNS access to CCR2hi monocytes and the generation of pathogenic cells through GM-CSF released by CNS endothelial cells. *Proc Natl Acad Sci U S A.* 2018;115(6):E1194-E1203.

38. Yona S, Kim KW, Wolf Y, et al. Fate mapping reveals origins and dynamics of monocytes and tissue macrophages under homeostasis. *Immunity*. 2013;38(1):79-91.

39. Goldmann T, Wieghofer P, Müller PF, et al. A new type of microglia gene targeting shows TAK1 to be pivotal in CNS autoimmune inflammation. *Nat Neurosci*. 2013;16(11):1618-26.

40. Goldmann T, Wieghofer P, Jordão MJ, et al. Origin, fate and dynamics of macrophages at central nervous system interfaces. *Nat Immunol*. 2016;17(7):797-805.

41. Pickering M, O'Connor JJ. Pro-inflammatory cytokines and their effects in the dentate gyrus. *Prog Brain Res*. 2007;163:339-54.

42. Chen Z, Jalabi W, Hu W, et al. Microglial displacement of inhibitory synapses provides neuroprotection in the adult brain. *Nat Commun*. 2014;5:4486.

43. Weinhard L, di Bartolomei G, Bolasco G, et al. Microglia remodel synapses by presynaptic trogocytosis and spine head filopodia induction. *Nat Commun*. 2018;9(1):1228.

44. Wen H, Gris D, Lei Y, et al. Fatty acid-induced NLRP3-ASC inflammasome activation interferes with insulin signaling. *Nat Immunol*. 2011;12(5):408-15.

45. Nagareddy PR, Kraakman M, Masters SL, et al. Adipose tissue macrophages promote myelopoiesis and monocytosis in obesity. *Cell Metab*. 2014;19(5):821-35.

46. Konsman JP, Tridon V, Dantzer R. Diffusion and action of intracerebroventricularly injected interleukin-1 in the CNS. *Neuroscience*. 2000;101(4):957-67.

47. Derecki NC, Cardani AN, Yang CH, et al. Regulation of learning and memory by meningeal immunity: a key role for IL-4. J Exp Med. 2010 May 10;207(5):1067-80.

48. Syková E. Extrasynaptic volume transmission and diffusion parameters of the extracellular space. *Neuroscience*. 2004;129(4):861-76.

49. Serrats J, Schiltz JC, García-Bueno B, van Rooijen N, Reyes TM, Sawchenko PE. Dual roles for perivascular macrophages in immune-to-brain signaling. *Neuron*. 2010;65(1):94-106.

50. Audoy-Rémus J, Richard JF, Soulet D, Zhou H, Kubes P, Vallières L. Rod-Shaped monocytes patrol the brain vasculature and give rise to perivascular macrophages under the influence of proinflammatory cytokines and angiopoietin-2. *J Neurosci*. 2008;28(41):10187-99.

51. Cunningham ET Jr, Wada E, Carter DB, Tracey DE, Battey JF, De Souza EB. In situ histochemical localization of type I interleukin-1 receptor messenger RNA in the central nervous system, pituitary, and adrenal gland of the mouse. *J Neurosci*. 1992;12(3):1101-14.

52. Srinivasan D, Yen JH, Joseph DJ, Friedman W. Cell type-specific interleukin-1beta signaling in the CNS. *J Neurosci*. 2004;24(29):6482-8.

53. Liu X, Yamashita T, Chen Q, et al. Interleukin 1 type 1 receptor restore: a genetic mouse model for studying interleukin 1 receptor-mediated effects in specific cell types. *J Neurosci*. 2015;35(7):2860-70.

54. Huang Y, Smith DE, Ibáñez-Sandoval O, Sims JE, Friedman WJ. Neuron-specific effects of interleukin-1β are mediated by a novel isoform of the IL-1 receptor accessory protein. *J Neurosci*. 2011;31(49):18048-59.

55. Smith DE, Lipsky BP, Russell C, et al. A central nervous system-restricted isoform of the interleukin-1 receptor accessory protein modulates neuronal responses to interleukin-1. *Immunity*. 2009;30(6):817-31.

56. Prieto GA, Snigdha S, Baglietto-Vargas D, et al. Synapse-specific IL-1 receptor subunit reconfiguration augments vulnerability to IL-1β in the aged hippocampus. *Proc Natl Acad Sci U S A*. 2015;112(36):E5078-87.

57. Katsuki H, Nakai S, Hirai Y, Akaji K, Kiso Y, Satoh M. Interleukin-1 beta inhibits long-term potentiation in the CA3 region of mouse hippocampal slices. *Eur J Pharmacol*. 1990;181(3):323-6.

58. Kelly A, Lynch A, Vereker E, et al. The anti-inflammatory cytokine, interleukin (IL)-10, blocks the inhibitory effect of IL-1 beta on long term potentiation. A role for JNK. *J Biol Chem*. 2001;276(49):45564-72.

59. Lynch MA. Neuroinflammatory changes negatively impact on LTP: A focus on IL-1β. *Brain Res*. 2015;1621:197-204.

60. Vereker E, O'Donnell E, Lynch MA. The inhibitory effect of interleukin-1beta on long-term potentiation is coupled with increased activity of stress-activated protein kinases. *J Neurosci.* 2000;20(18):6811-9.

61. Avital A, Goshen I, Kamsler A, et al. Impaired interleukin-1 signaling is associated with deficits in hippocampal memory processes and neural plasticity. *Hippocampus*. 2003;13(7):826-34.

62. Biancardi VC, Stranahan AM, Krause EG, de Kloet AD, Stern JE. Cross talk between AT1 receptors and Toll-like receptor 4 in microglia contributes to angiotensin II-derived ROS production in the hypothalamic paraventricular nucleus. *Am J Physiol Heart Circ Physiol*. 2016;310(3):H404-15.

63. Wang Q, Rowan MJ, Anwyl R. Beta-amyloid-mediated inhibition of NMDA receptor-dependent long-term potentiation induction involves activation of microglia and stimulation of inducible nitric oxide synthase and superoxide. *J Neurosci*. 2004;24(27):6049-56.

64. Wosiski-Kuhn M, Erion JR, Gomez-Sanchez EP, Gomez-Sanchez CE, Stranahan AM. Glucocorticoid receptor activation impairs hippocampal plasticity by suppressing BDNF expression in obese mice. Psychoneuroendocrinology. 2014;42:165-77.

65. Fotuhi M, Hachinski V, Whitehouse PJ. Changing perspectives regarding late-life dementia. *Nat Rev Neurol*. 2009;5(12):649-58.

66. Bos I, Vos SJ, Frölich L, et al. The frequency and influence of dementia risk factors in prodromal Alzheimer's disease. *Neurobiol Aging*. 2017;56:33-40.

67. Gu Y, Brickman AM, Stern Y, et al. Mediterranean diet and brain structure in a multiethnic elderly cohort. *Neurology*. 2015;85(20):1744-51.

68. Hillman CH, Erickson KI, Kramer AF. Be smart, exercise your heart: exercise effects on brain and cognition. *Nat Rev Neurosci*. 2008;9(1):58-65.

69. Handley JD, Williams DM, Caplin S, Stephens JW, Barry J. Changes in Cognitive Function Following Bariatric Surgery: a Systematic Review. *Obes Surg*. 2016;26(10):2530-7.

70. Marques EL, Halpern A, Corrêa Mancini M, et al. Changes in neuropsychological tests and brain metabolism after bariatric surgery. *J Clin Endocrinol Metab*. 2014;99(11):E2347-52.

71. Hawkins MA, Alosco ML, Spitznagel MB, et al. The Association Between Reduced Inflammation and Cognitive Gains After Bariatric Surgery. *Psychosom Med*. 2015 Jul-Aug;77(6):688-96.

72. Fabbrini E, Tamboli RA, Magkos F, et al. Surgical removal of omental fat does not improve insulin sensitivity and cardiovascular risk factors in obese adults. *Gastroenterology*. 2010;139(2):448-55.

73. Dunn JP, Abumrad NN, Breitman I, et al. Hepatic and peripheral insulin sensitivity and diabetes remission at 1 month after Roux-en-Y gastric bypass surgery in patients randomized to omentectomy. *Diabetes Care*. 2012;35(1):137-42.

74. Lee Y, Pędziwiatr M, Major P, Brar K, Doumouras AG, Hong D. The effect of omentectomy added to bariatric surgery on metabolic outcomes: a systematic review and meta-analysis of randomized controlled trials. *Surg Obes Relat Dis*. 2018;14(11):1766-1782.

75. Erion JR, Wosiski-Kuhn M, Dey A, et al. Obesity elicits interleukin 1-mediated deficits in hippocampal synaptic plasticity. *J Neurosci*. 2014;34(7):2618-31.

76. Stranahan AM, Arumugam TV, Cutler RG, Lee K, Egan JM, Mattson MP. Diabetes impairs hippocampal function through glucocorticoid-mediated effects on new and mature neurons. *Nat Neurosci*. 2008;11(3):309-17.

77. Stranahan AM, Lee K, Becker KG, et al. Hippocampal gene expression patterns underlying the enhancement of memory by running in aged mice. *Neurobiol Aging*. 2010;31(11):1937-49.

78. Banks WA, Ortiz L, Plotkin SR, Kastin AJ. Human interleukin (IL) 1 alpha, murine IL-1 alpha and murine IL-1 beta are transported from blood to brain in the mouse by a shared saturable mechanism. *J Pharmacol Exp Ther*. 1991;259(3):988-96.

79. Dey A, Hao S, Erion JR, Wosiski-Kuhn M, Stranahan AM. Glucocorticoid sensitization of microglia in a genetic mouse model of obesity and diabetes. *J Neuroimmunol*. 2014;269(1-2):20-7.

Figures and Figure Legends

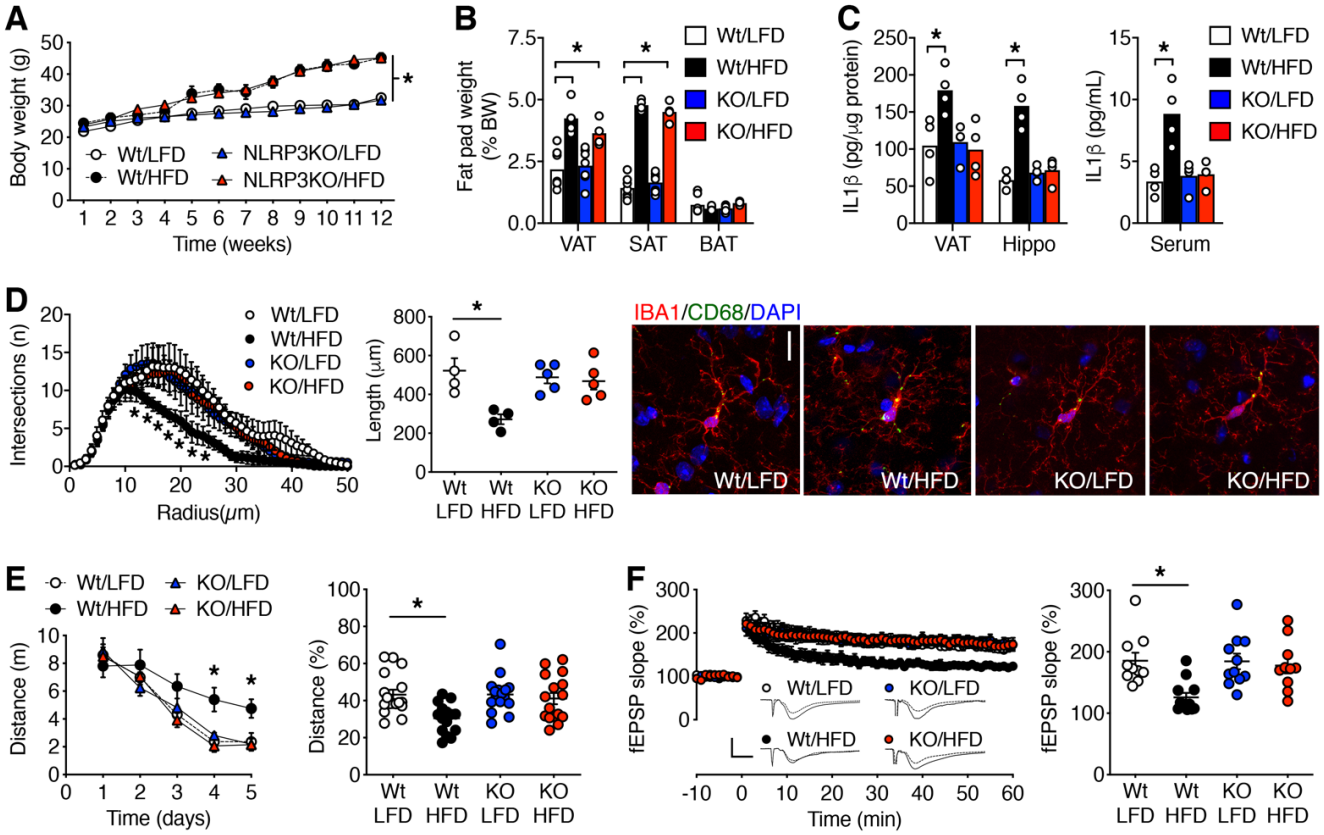

Figure 1. Protection against obesity-induced hippocampal dysfunction in mice lacking inflammasome protein NLRP3. (A) Male Wt and NLRP3 knockout (KO) mice gain weight similarly over time (n=20). (B) Adipose tissue hypertrophy is comparable in Wt/HFD and KO/HFD mice (n=6). (C) KO/HFD mice are protected against increases in IL1β in VAT, hippocampus, and serum (n=4). (D) NLRP3-dependent reductions in microglial process complexity (left) and total length (right) with dietary obesity (n=4). Micrographs (right; scale bar = 10 microns, applies to all panels) show increased CD68 immunoreactivity in Wt, but not KO/HFD mice (see Supplemental Figure 1). (E) NLRP3 is required for obesity-induced memory impairment in the water maze during acquisition training (left) and probe test (right; n=16). (F) Dentate gyrus long-term potentiation (LTP) was significantly reduced in an NLRP3-dependent manner with dietary obesity (n=10-12 slices, n=4-6 mice). For traces (inset, left), scalebar x=1msec, y=1mV. For all graphs, bar or line height represents the mean and error bars represent SEM. Asterisk (*) denotes statistical significance at $p<0.05$ by 2-way repeated-measures ANOVA (A) or 2-way ANOVA (B-F) with Tukey's HSD post hoc.

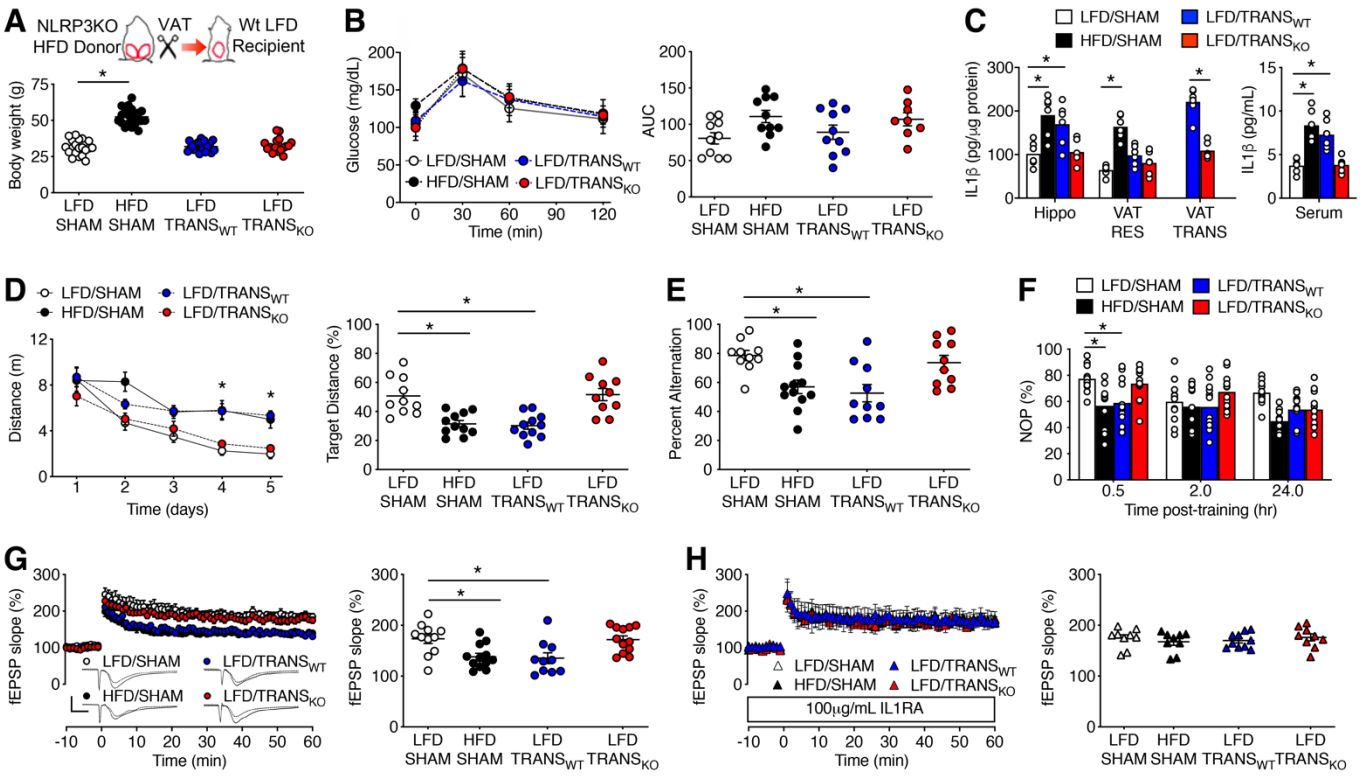

Figure 2. Visceral adipose NLRP3 induction impairs hippocampus-dependent memory and synaptic plasticity. (A) Top panel shows experiment schematic. Bottom graph shows body weights in Wt mice maintained on HFD or LFD for 10wk before sham operation (SHAM) or VAT transplantation from a Wt/HFD (TRANS$_{WT}$) or NLRP3KO/HFD donor (TRANS$_{KO}$) (n=20). (B) No effect of VAT transplantation on glycemic control, as determined by IPGTT (left) and analysis of the area under the curve (AUC, right; n=8-10). (C) Increases in hippocampal and serum IL1β in HFD/SHAM and TRANS$_{WT}$ mice, but not TRANS$_{KO}$ mice (n=6). (D) Visceral adipose NLRP3 impairs spatial memory acquisition (left) and probe trial performance (right; n=10-11). (E) NLRP3-mediated deficits in the Y-maze following VAT transplantation (n=10-12). (F) NLRP3-dependent reductions in novel object preference (NOP) (n=12). (G) TRANS$_{WT}$ mice recapitulate obesity-induced LTP deficits in an NLRP3-dependent manner (left), based on comparison of fEPSP slopes 60min after high-frequency stimulation (n=9-10 slices, n=4-5 mice). For traces (left inset), scalebar x=1msec, y=1mV. (H) Recombinant interleukin-1 receptor antagonist (IL1RA) eliminated LTP deficits in TRANS$_{WT}$ mice (n=9-10 slices, n=4-5 mice). For all graphs, bar or line height represents the mean and error bars represent SEM. Asterisk (*) denotes statistical significance at $p<0.05$ by one-way ANOVA with Tukey's HSD post hoc.

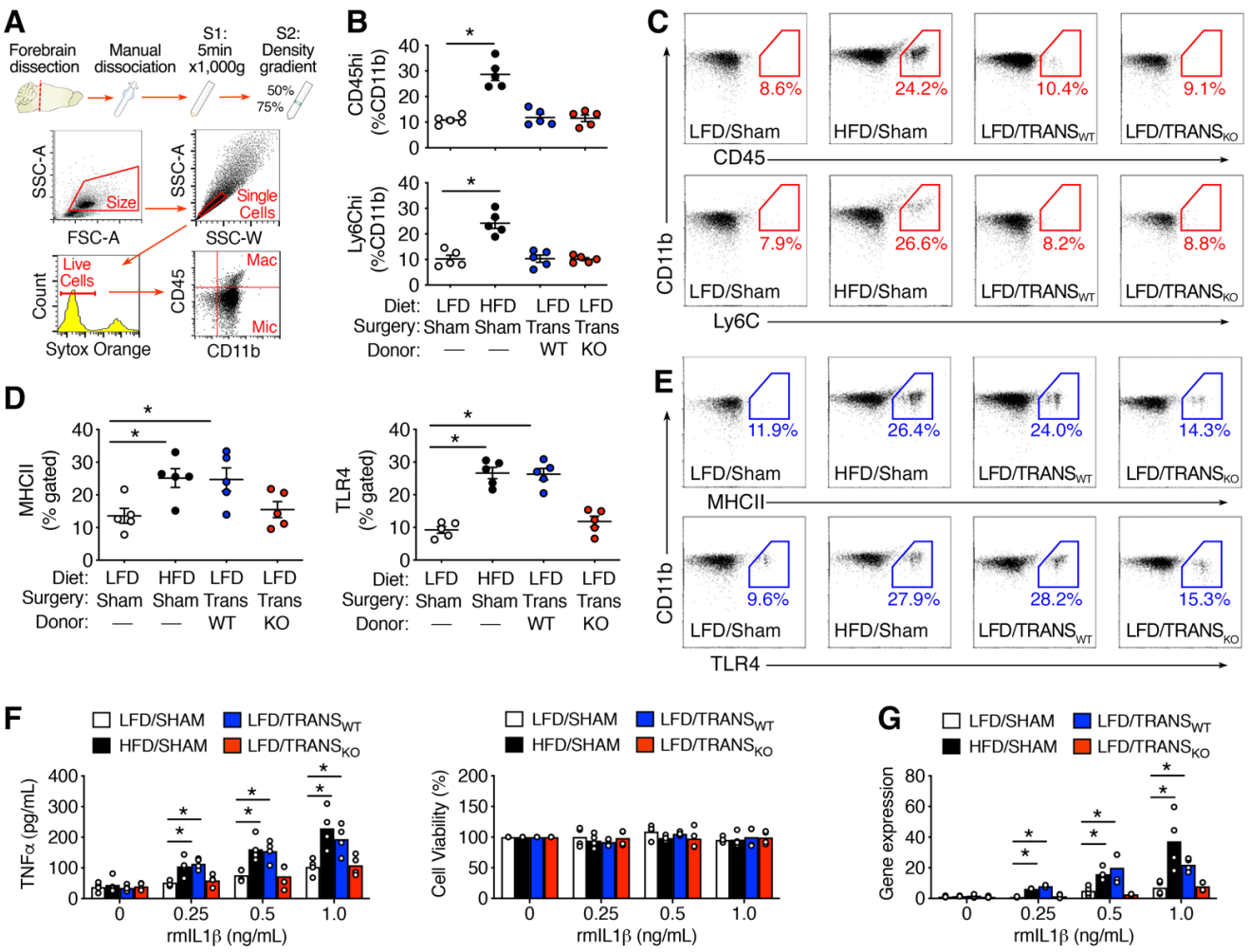

Figure 3. NLRP3-mediated effects of visceral fat transplantation on forebrain microglia. (A) Top panel shows schematic of cell isolation; bottom panel shows gating. (B) Visceral fat transplantation does not recapitulate obesity-induced macrophage infiltration (n=5). (C) Representative scatterplots of CD11b+/CD45hi cells (top) and CD11b+/Ly6Chi cells (bottom). Boxed area (red) shows gated events. (D) VAT transplantation recapitulates the effect of obesity on microglial induction of MHCII (left) and TLR4 (right) via NLRP3 (n=5). (E) Representative scatterplots of MHCII (top) and TLR4 (bottom) in CD11b+ cells. Boxed area (blue) shows gated events. For all scatterplots (C, E) XY axis (log scale) min=10^0, max=10^5. (F) Visceral adipose NLRP3 increases sensitivity to exogenous IL1β in forebrain mononuclear cells (left) without influencing cell viability (right; n=4). (G) NLRP3-mediated priming of IL1β-stimulated gene expression with dietary obesity or VAT transplantation (n=4). For all graphs, bar or line height represents the mean and error bars represent SEM. Asterisk (*) denotes statistical significance at $p<0.05$ by one-way ANOVA with Tukey's HSD post hoc.

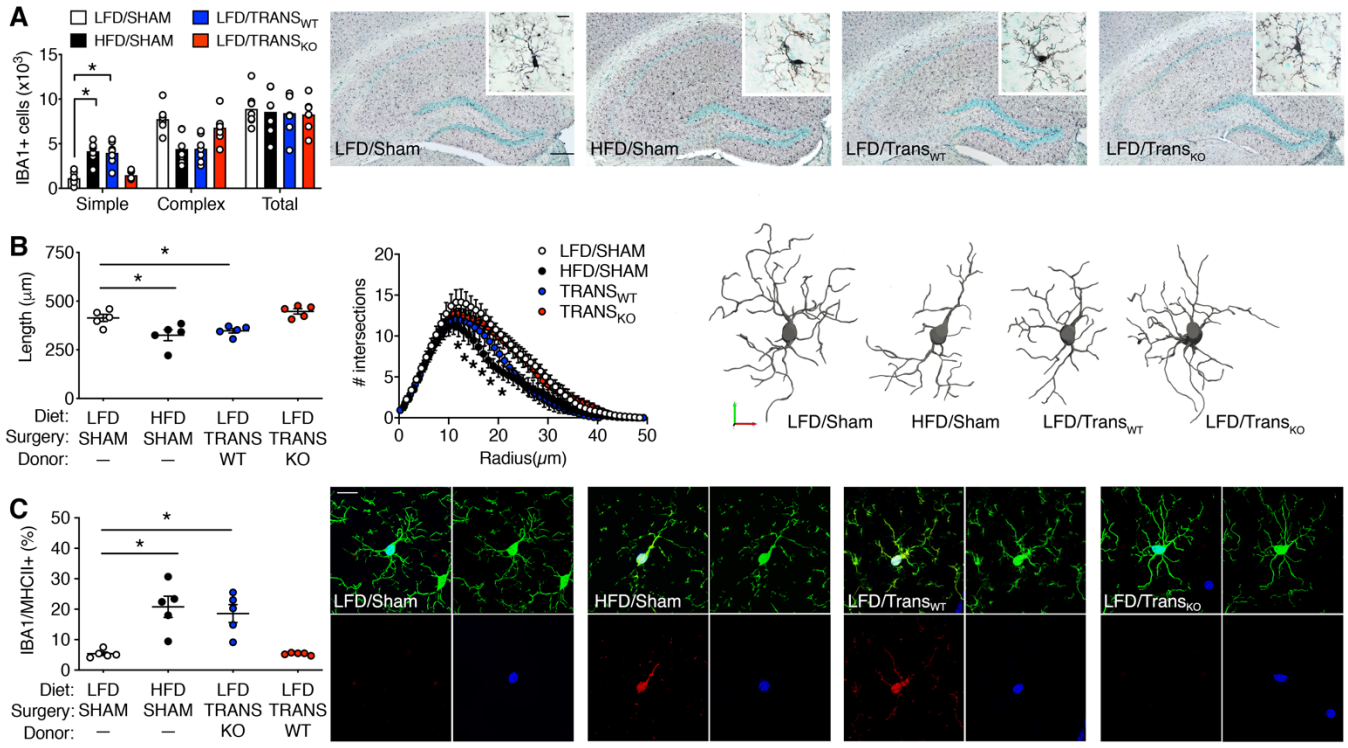

Figure 4. Visceral adipose NLRP3 induction activates hippocampal microglia in the intact brain. (A) Stereological quantification of IBA1+ microglia with ≤2 primary processes ('Simple'), >2 primary processes ('Complex'), and total microglial number (n=7). Micrographs (right; scale bar = 5mm; for inset, scale bar = 10 microns) show peroxidase detection of IBA1. (B) Quantification of total process length (left) and complexity (right) revealed NLRP3-dependent simplification of IBA1+ microglia after VAT transplantation (n=5). For tracings (right), scalebar for LFD/SHAM applies to all tracings (xyz=5 micron). (C) VAT transplantation recapitulated the effects of obesity on microglial MHCII induction via NLRP3 (n=5). Micrographs (right; scale bar = 10 microns) show double-labeling for IBA1 and MHCII in the hippocampal dentate gyrus. For micrographs, scale bar shown for LFD/SHAM applies to all panels. For all graphs, bar or line height represents the mean and error bars represent SEM. Asterisk (*) denotes statistical significance at $p<0.05$ by one-way ANOVA with Tukey's post hoc.

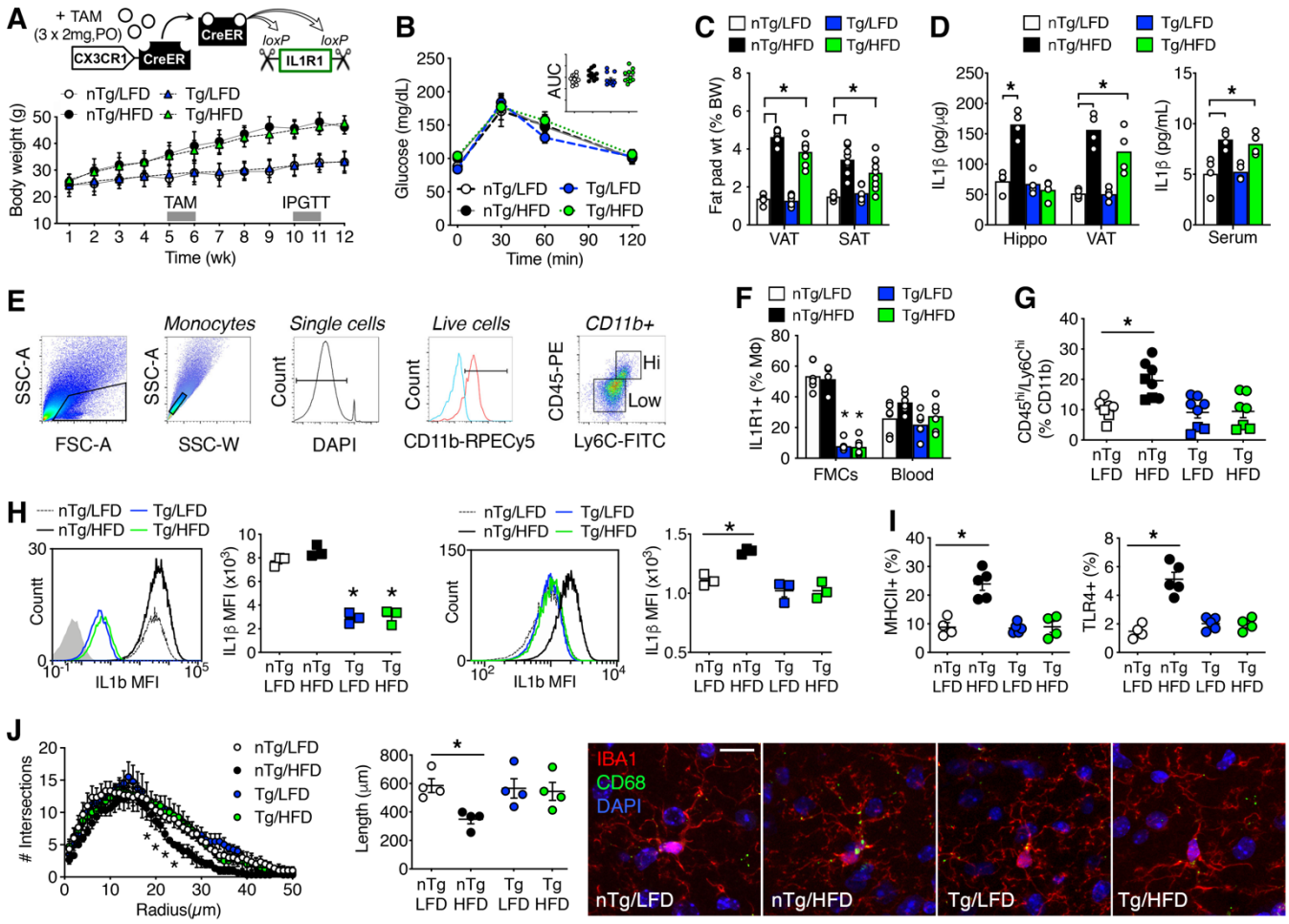

Figure 5. Ablation of IL1R1 in CX3CR1-expressing cells confers resistance to obesity-induced neuroinflammation. (A) Top panel shows design for CX3CR1$^{cre/ERT2}$/IL1R1$^{fl/fl}$ transgenic mice. Weight gain (bottom) is similar in Tg and nTg littermates (n=24). (B) No effect of genotype on glycemic control (n=11-12). (C) Adipose tissue hypertrophy is unaffected by genotype (n=6-8). (D) Tg/HFD mice did not exhibit increases in hippocampal IL1β, despite comparable increases in VAT and serum IL1β (n=4). (E) Gating strategy for analysis of macrophage infiltration and microglial activation (text above plots indicates parent gate). (F) Flow cytometric validation of CNS-specific reductions in cell-surface IL1R1 expression (n=6). (G) Tg mice are resistant to CNS infiltration of CD11b+/CD45^{hi}/Ly6C^{hi} macrophages with dietary obesity (n=7-8; circles show data from cell-surface detection in live cells (n=4-5) and squares represent data from fixed cells (n=3). (H) Nonoverlapping effects of obesity and IL1R1 deletion on intracellular IL1β in the CD11b+/CD45^{hi}/Ly6C^{low} population, which includes BAMs (right; gray region shows isotype) and in CD11b+/CD45^{low}/Ly6C^{low} microglia (left; n=3). (I) IL1R1 is required for obesity-induced microglial polarization, based on cell-surface detection of MHCII (left) and TLR4 (right) in CD11b+/CD45^{low}/Ly6C^{low} cells (n=4-5). (J) IL1R1-dependent anatomical simplification (left) and process retraction (right) with obesity (n=4). Micrographs show IL1R1-mediated accumulation of CD68 among IBA1+ microglia (scale bar=10 microns, applies to all). For all graphs, bar or line height represents the mean and error bars show SEM. Asterisk (*) denotes statistical significance at $p<0.05$ by 2-way ANOVA with Tukey's post hoc.

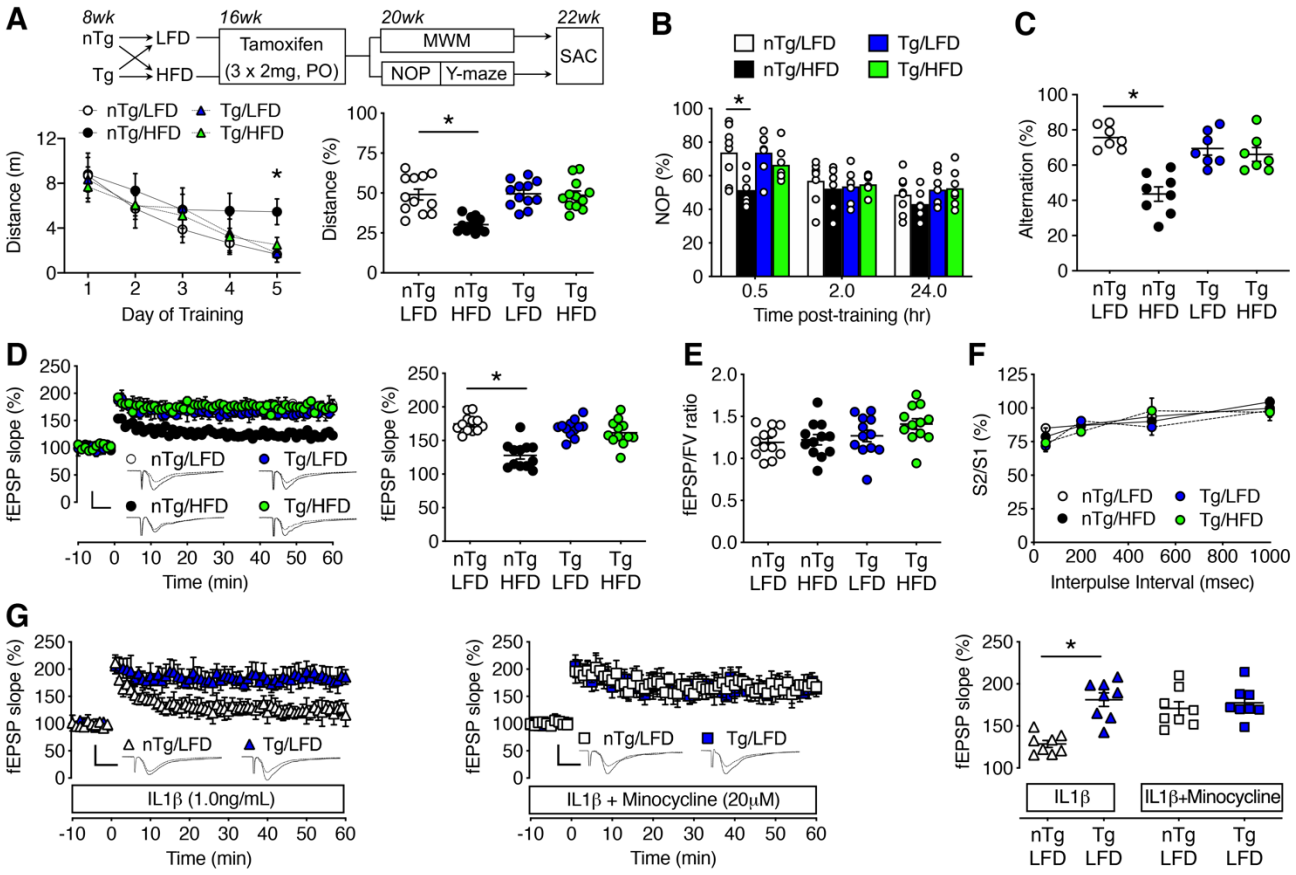

Figure 6. Protection against obesity-induced hippocampal dysfunction in CX3CR1^{creERT}/IL1R1$^{fl/fl}$ mice. (A) Top panel shows experiment schematic (italics indicate age of mice). Bottom graphs show distance during water maze acquisition (left) and probe test (right; n=12). (B) IL1R1 activation in CX3CR1-expressing cells impairs object recognition in obesity (n=6-8). (C) Ablation of IL1R1 in CX3CR1-expressing cells eliminates deficits in the Y-maze with dietary obesity (n=7-8). (D) Activation of IL1R1 in CX3CR1-expressing cells underlies obesity-induced LTP deficits (n=12 slices, n=5-6 mice; applies to panels D-F). For traces (inset, left), scalebar x=1msec, y=1mV. (E) No effect of diet or genotype on input/output ratios. (F) No effect of diet or genotype on paired-pulse depression. (G) Inducible ablation of IL1R1 among CX3CR1-expressing cells protects against IL1β-induced LTP deficits (left). Preincubation with minocycline blocks reductions in LTP with exposure to IL1β in slices from nTg mice (middle graph). Right graph shows normalized fEPSP slopes 60min after high-frequency stimulation (n=8 slices from n=4 mice per condition). For all graphs, bar or line height represents the mean and error bars show SEM. Asterisk (*) denotes significance at $p<0.05$ by 2-way ANOVA with Tukey's HSD post hoc.

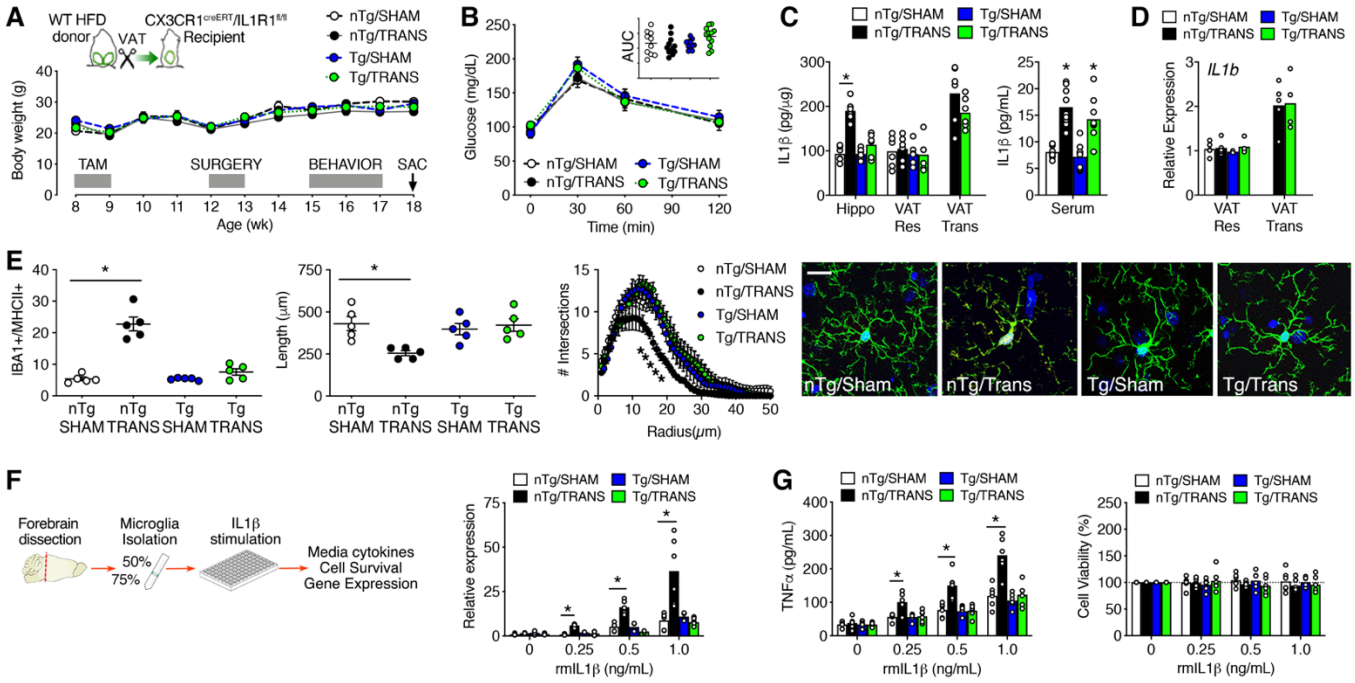

Figure 7. Inducible ablation of IL1R1 in CX3CR1-expressing cells prevents microglial activation and sensitization following surgical increases in visceral fat. (A) Top panel shows experiment schematic. Graph (bottom) shows weight gain after VAT transplantation (TRANS) or sham operation (SHAM) in CX3CR1$^{cre/ERT2}$/IL1R1$^{fl/fl}$ transgenic mice (Tg) and nTg littermates (n=32). (B) No effect of genotype or surgery on glycemic control (n=12). (C) Visceral fat transplantation increases hippocampal IL1β in nTg mice, but not in Tg mice, despite comparable elevations in serum IL1β (n=6). (D) qPCR analysis of IL1b demonstrating localized increases in the transplanted VAT (n=4-5). (E) IL1R1-dependent MHCII induction in IBA1+ cells after VAT transplantation (left). IL1R1-mediated reductions in total process length (middle) and complexity (right) in VAT transplant recipients (n=5). Micrographs show MHCII expression in IBA1+ cells (scale bar=10 microns, applies to all). (F) Schematic (left) shows experimental design for analysis of priming and sensitization (n=6). Graph (right) shows IL1R1-mediated autocrine amplification of IL1b gene expression in FMCs after VAT transplantation. (G) FMCs from VAT transplant recipients exhibit IL1R1-dependent sensitization, based on lower thresholds for increases in media TNFa (left). Sensitization and priming were not attributable to differences in cell survival (right; n=6). For all graphs, bar or line height represents the mean, error bars show SEM, and n-sizes represent number of mice. Asterisk (*) denotes statistical significance at $p<0.05$ by 2-way ANOVA with Tukey's HSD post hoc.

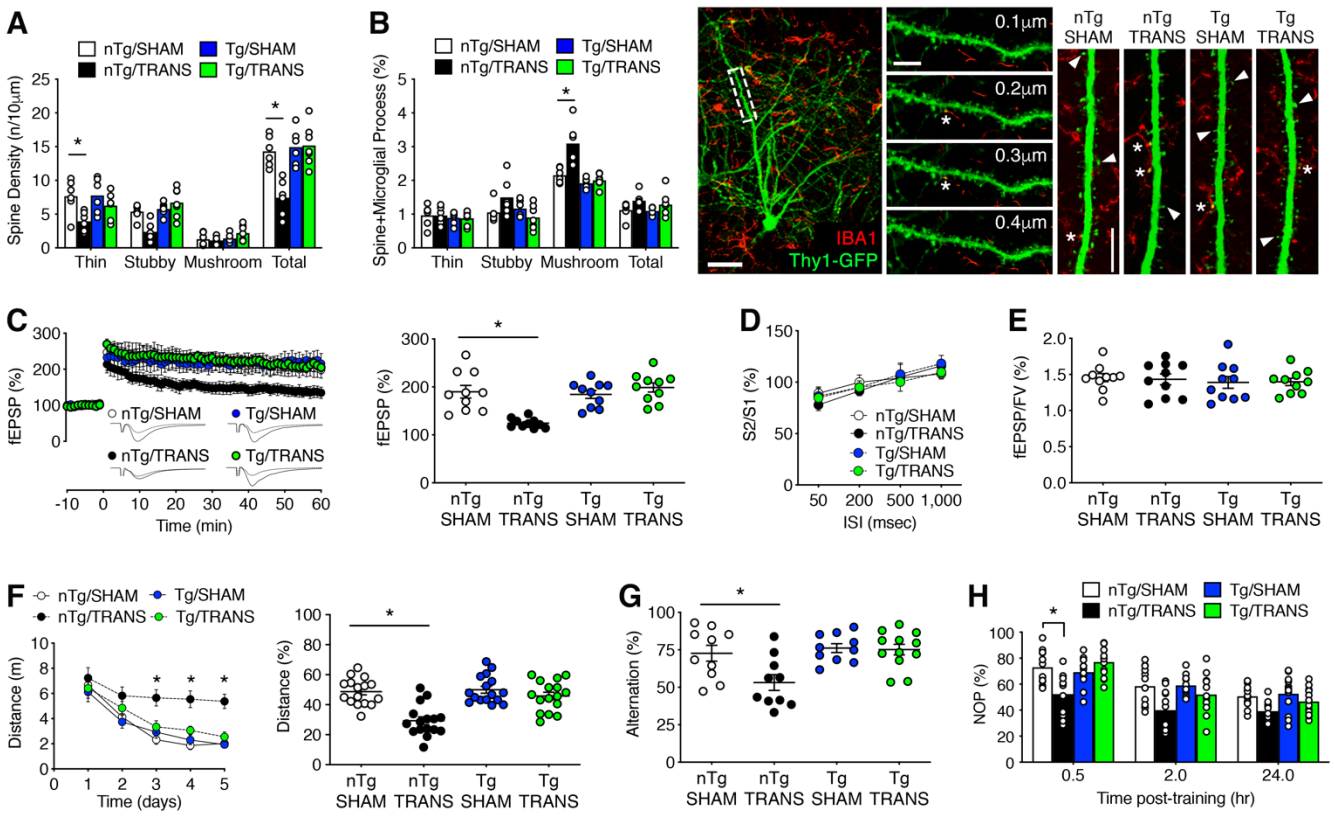

Figure 8. Visceral fat transplantation disrupts microglial organization at dendritic spines and impairs cognition by activating IL1R1 on microglia and brain macrophages. (A) CX3CR1$^{cre/ERT}$/IL1R1$^{fl/fl}$ transgenic mice were crossed with Thy-eGFP(S) mice for quantification of dendritic spine density and morphology. Loss of thin spines was associated with reductions in total dendritic spine density in nTg/TRANS mice (n=6-7, applies to A-B). (B) Analysis of IBA1+ microglial processes at different spine morphologies revealed preferential localization at mushroom spines. VAT transplantation increased the proportion of mushroom spines with microglial processes, and increases were IL1R1-dependent. For micrographs, left panel shows z-projection of Thy1-GFP and IBA1 (scalebar = 20 microns); middle panels show individual z-planes with asterisk (*) indicating contact between IBA1+ processes and dendritic spines (scalebar = 10 microns). Far right panels show representative z-projection images from each condition with arrowheads indicating spines and asterisks indicating IBA1 contact at spine head (scalebar = 10 microns). (C) Protection against VAT transplantation-induced LTP deficits in Tg/TRANS (left), based on comparison of fEPSP slopes 60min after high-frequency stimulation (right; n=10 slices, n=4-5 mice, applies to D-E). (D) No change in presynaptic paired-pulse plasticity. (E) No effect of genotype or surgery on input/output ratios. (F) VAT transplantation impairs water maze acquisition (left) and probe trial performance (right) in nTg/TRANS, but not Tg/TRANS mice (n=16). (G-H) Ablation of IL1R1 in CX3CR1-expressing cells eliminates VAT transplantation-induced deficits in the Y-maze (G) and maintains object recognition memory (H; n=10-12, applies to G-H). For all graphs, bar or line height represents the mean and error bars show SEM. Asterisk (*) denotes statistical significance at $p<0.05$ by 2-way ANOVA with Tukey's HSD post hoc.